ZEUS Note 99-078
December 14, 1999

Proposal of an Upgraded Luminosity Monitor for the ZEUS Experiment

ZEUS Luminosity Group

J. Andruszków, J. Chwastowski, W. Daniluk, A. Eskreys, J. Figiel, P. Jurkiewicz, K. Klimek, A. Kotarba, J. Ligocki, K. Oliwa, K. Olkiewicz, M.B. Przybycień, P. Stopa, W. Wierba, L. Zawiejski

Institute of Nuclear Physics, Kraków

L. Adamczyk, D. Kisielewska, A. Kowal, L.Suszycki, D. Szuba

Faculty of Physics and Nuclear Techniques, University of Mining and Metallurgy, Kraków

Abstract

The upgraded luminosity monitor is proposed for the ZEUS experiment. It is an extension of the detection scheme of bremsstrahlung photons used so far by the ZEUS experiment. This monitor will stand the conditions after the upgrade of HERA i.e. nearly 7 fold increase of the flux of synchrotron radiation, 4 fold increase of its critical energy and ~ 5 fold increase of the rate of bremsstrahlung photons.

The monitor will consist of the active aerogel-carbon filter and sandwich lead-scintillator calorimeter with the inserted position detector. The role of the active filter is two fold: it screens the calorimeter and position detector from destruction and it serves either as the veto counter or as the compensator of energy lost in the filter.

Three possible ways of determination of luminosity are discussed and the expected error on luminosity varies between 1.2% and 2.3%.

Contents

List of Figures

List of Tables

1 Introduction

The planned (during the year 2000) upgrade of the HERA collider aiming at the increase of the delivered luminosity to a value of $7 \cdot 10^{31}$ cm^{-2}s^{-1}, essentially by the modification of the beam geometry, will have two basic consequences for the measurement of luminosity based on counting the bremsstrahlung photons:

- the increase of the flux and hardness of the synchrotron radiation
  and
- the increase of the bremsstrahlung events rate.

If we stick to the present concept of the luminosity measurement [1, 2, 3] then the positioning of the bremsstrahlung photon detector will not change and the window to let these photons out of the proton beam pipe will stay at 92.5 m from the I.P.

In further, we shall discuss the impact of the mentioned consequences on the luminosity measurement.

1.1 Synchrotron radiation

Both, the flux of the synchrotron photons and their critical energy will increase.

In Table 1 the present conditions at the γ exit window are compared with those expected after upgrade assuming two different electron beam energies: 27.5 GeV and 30 GeV.

	Present	Upgrade	
E_{beam} (GeV)	27.5	27.5	30
ρ (m) - radius of bending	1360	400	400
I_e (mA)	43	58	58
Energy (GeV/bcr)	0.165×10^6	0.76×10^6	1.07×10^6
Power (W)	275	1260	1785
Critical energy (keV)	34	115	150

Table 1: Synchrotron radiation at the γ-exit window. (Angle in horizontal plane = 1.08 mrad.)

In Table 1 we consider two scenarios after the upgrade: the optimistic one for energy of the electron beam of 27.5 GeV and the pessimistic one for the beam energy of 30 GeV, both assuming bending radius of 400 m i.e. the field of bending magnet B=0.25 T. With the presently planned increase of B to the value of 0.274 T but the beam energy close to 27.5 GeV we think that the reality will be somewhere in between the two scenarios. In Table 2 [4] we quote the numbers for dissipation of energy in different equipment placed behind the γ exit and calorimeter, assuming total flux of the synchrotron photons of 1800 W (unfavorable scenario).

Note that the dissipation of energy by the scattered photons is sizable - indeed they scatter in the window, in the vacuum pipe and all other equipment on their way to calorimeter.

As an illustration let us consider the total energy carried by the flux of synchrotron photons. This energy will be dissipated in the materials sitting on their way - it will increase from 275 W at present to $\sim$ 1800 W after upgrade, assuming 30 GeV electron beam after upgrade. As an example the MC estimation of energy dissipation in various elements on the way to calorimeter is calculated for 3 thicknesses of the copper window - see table 2.

Cu γ window thickness/obstacle			
	0.15 cm	0.30 cm	0.45 cm
window	630 W	800 W	930 W
lumi vacuum pipe	40 W	18 W	15 W
scattered	570 W	510 W	460 W
filter	580 W	460 W	390 W
sum	1800 W	1800 W	1800 W

Table 2: Synchrotron radiation heat dissipation

The quoted values correspond to the different thickness of the Cu γ exit window (0.15 - 0.45) cm. Judging from these numbers one sees that the γ exit window must be cooled (by water) while cooling of the filter by a fan should be probably sufficient but should be studied in more details.

It is also obvious, that if one wants to use the present luminosity measurement concept (filter + sandwich type absorber/scintillator calorimeter), one needs a thicker filter to screen the calorimeter from destruction and to enable the distinction of the signal (bremsstrahlung photons) from the background (synchrotron radiation). Irrespectively of that a radiation resistive scintillator has to be used in calorimeter. The synchrotron photons can be removed by a filter since they are much softer than the bremsstrahlung photons (Fig.1).

A detailed MC simulations were performed [5] by generating the synchrotron photons in the energy interval (50 - 1500) keV - below 50 keV photons will be totally absorbed even in the thin filter ($\sim$ $2X_0$ thickness) while above 1500 keV there is a negligible number of them. These simulations show that after $4X_0$ thick filter the deposit from the synchrotron radiation in a calorimeter of the lead-scintillator sandwich type of $24X_0$ depth will be 0.04 of that from the 10 GeV bremsstrahlung photon. The expected doses from both the synchrotron radiation and from the bremsstrahlung are compared in Table 3. After $4X_0$ filter the contribution from the synchrotron radiation will shift the PM's pedestals by $\sim$ 0.4 GeV up with the spread of $\sim$(0.2 - 0.3) GeV. With this filter the total radiation dose from the bremsstrahlung itself will be $\sim$ 1.1 Mrad/year while that from the synchrotron radiation $\sim$0.10 Mrad/year.

The total deposit from the bremsstrahlung photons was calculated assuming the total delivered luminosity after upgrade of 181.75 pb^{-1}/yr. This last number has been estimated

	1997	Upgrade [6]
L_{inst}(peak)	1.4×10^{31} cm^{-2}s^{-1}	7×10^{31} cm^{-2}s^{-1}
L_{integr}(delivered)	36.35 pb^{-1}/yr	$\sim$ 181.75 pb^{-1}/yr

After upgrade		
	Synchrotron radiation	Bremsstrahlung
MC results	0.04 GeV/bcr	0.50 GeV/event ($\equiv$ 0.38 GeV/bcr)
Estimated one year deposit	2.85×10^{12} GeV	1.0×10^{13} GeV
Irradiated area	4 cm $\times$ 12 cm = 48 cm^2	$\pi \times$ 2 cm $\times$2.4 cm = 15 cm^2
Total scintillator length	48 $\times$ 0.2 = 9.6 cm	48 $\times$ 0.2 = 9.6 cm
Irradiated mass	475 g	148 g
Average dose per year	991 Gy = 0.10 Mrad	11 kGy = 1.1 Mrad

Table 3: Radiation doses in the LUMI calorimeter.

by rescaling the best so far achieved lumi of 36.3 pb^{-1}/yr in 1997. Then the dose was calculated following the steps shown in Table 3.

The dose from the synchrotron radiation was calculated assuming the photon exit window of 1 cm Al, critical energy of 126 keV and exposure of $\sim$ 1900 hours/yr (estimate made on the basis of '97 running experience).

The same MC simulation shows that the deposits from synchrotron radiation is concentrated mainly in the first two scintillator layers of the calorimeter. Fig.2 which is based on a rather low statistics MC shows however that the synchrotron photons can penetrate quite deep into the calorimeter.

Thus, the $4X_0$ filter is sufficient for both screening the calorimeter from the destruction and discriminate the signal from background.

However, it is known that the thicker is the filter the less reliable is the calorimeter energy measurement. As it will be shown in the next section the presence of $4X_0$ filter in front of the calorimeter will deteriorate its energy resolution from $\sim 30\%/\sqrt{E}$ to $\sim 90\%/\sqrt{E}$.

The only way out of this problem is to measure the energy loss in the filter and to correct the calorimeter deposit for this loss. This lead us to the idea of using an active filter i.e. the one which could measure the deposited energy. The inspection of the properties of available materials points towards the silica aerogel of a new generation [7] as an active material. The filter built of interlayed blocks of an carbon absorber and active aerogel material should do the job - see the section 2 for the detailed discussion.

1.2 Rate of bremsstrahlung photons

The rate of bremsstrahlung photons is proportional to the luminosity. Beside that the increase of this rate will contribute to the faster destruction of the detectors it creates a problem of a large probability of observing more than 1 bremsstrahlung photon in a single bunch crossing - so called pile-up effect.

The total expected rate of bremsstrahlung photons depends on the trigger used and for the maximum expected luminosity of $7.4 \cdot 10^{31} cm^{-2} s^{-1}$ will be [4]:

$E_\gamma > (trigger)$	3	5	10	GeV
σ_{BH}	105	74	40	mb
Rate	7.8	5.5	3.0	MHz

The expected multiplicity of bremsstrahlung photons/bcr is displayed in Fig.3 for 4 values of luminosity. The consequence of the increase of the multiple bremsstrahlung probability/bcr is clearly seen in Fig.4, where the expected bremsstrahlung photons energy spectra are displayed. With the increase of luminosity a high energy tail develops. This in turn leads to the modification of the method of fitting the energy distribution observed in calorimeter and estimation of the luminosity [8] - see section 6.

Another effect of developing the high energy tail is the necessity of using the higher accuracy FADC converters in order to achieve the sufficient precision in the FADC measurement. We have chosen the 12 bits converters, which for the expected measured energy interval (0.1 - 100) GeV assure the accuracy of $\sim$ 50 MeV, being well below the attainable energy resolution of the detector, even for the low energy photons ($E_\gamma \sim 0.1$ GeV).

However, if one sticks to the luminosity measurement based on counting the bunch crossings with energy of emitted photons above certain threshold, one can prove by MC simulation that for each luminosity exists the threshold energy for which the effects of pile-up cancels out. This threshold energies are weakly dependent on luminosity.

In Fig.5 the ratio of the number of bcr (N_b) to the number of generated photons (N_γ), both with the energy above the threshold is plotted as a function of the threshold energy for 4 different luminosities. The curves for each luminosity cross the value $N_b/N_\gamma = 1$ at certain threshold energy, indicating that at this threshold value the pile-up effects cancel. Canceling of pile-up effect means that as much photons we loose (there are 2 or more photons in bcr with energies above threshold but counted as one) as we gain (there are 2 or more photons, each below threshold but the sum of their energy is above threshold but again counted as one).

Finally, the beam-gas collisions are relatively free from the pile-up effects since their rate is rather low and it will probably stay low after the upgrade (the electron beam current will not increase much and the vacuum will stay essentially the same as at present).

Additionally the beam-gas collisions are free from the beam-size effects [9] and therefore it is tempting to use them for calibration purposes.

2 Aerogel as the active material for filter

A sample of 20 silicon aerogel plates ($11 \times 11 \times 1$) cm^3 were purchased in the Japanese firm [10] for the purpose to test its properties and applicability for the active filter in the conditions of running the luminosity monitor after the HERA upgrade.

This material is radiation resistant and emits the Čerenkov light when the charged particle passes through it. The properties of the tested aerogel are listed in Table 4.

size	($11 \times 11 \times 1$) cm^3
density	0.11 g/cm^3
refraction index	1.03
transparency at 400 nm	> 80 %/cm
radiation resistance	> 10 Mrad

Table 4: Properties of tested aerogel

The simulations of synchrotron background in aerogel were made for the two extreme cases of electron beam energy of 27.5 GeV and 30 GeV.

A synchrotron photon can lead to Č photon emission in aerogel only through Compton effect and this requires that its kinetic energy exceeds 1.6 MeV.[1] Since even for high critical energy, such synchrotron photons are rather rare, their background is expected to be small.

In Table 5 the number of expected Č photons generated in aerogel/cm/bcr are given for the two energies and various thicknesses of filter, sitting in front of the first stack of aerogel.

Filter/E_{beam}	$0.5X_0$	$1.0X_0$	$1.5X_0$	$2.0X_0$	$2.5X_0$	$3.0X_0$
30 GeV	111	50	24	12.7	5.8	1.9
27.5 GeV	10	5.3	2.0	1.1	0.8	0.3

Table 5: The number of expected Č photons generated in aerogel/cm/bcr by synchrotron photons.

Assuming that the beam energy will be $28 \div 29$ GeV and our aerogel filter will sit after $2.3X_0$ ($0.3X_0$ - γ exit window, $2.0X_0$ - filter) ~ 3 Č synchrotron photons/cm/bcr are expected and should be compared with ~ 100 Č photons/cm/bcr from a 10 GeV bremsstrahlung photon.

[1]Note that a vast majority of such Compton electrons if produced inside the filter, will be absorbed in the filter.

2.1 Results of the aerogel tests at the DESY test beam

A series of tests of variable aerogel stack thickness were made both in the HERA tunnel and at the DESY 3 GeV $e^{\pm}$ test beams during which a considerable experience was gained. The recent tests were made in July '99 using a stack of 5 aerogel plates of properties listed in Table 4. During the earlier tests this thickness of aerogel was found optimal but will be checked again in the forthcoming tests.

The main problem in using the aerogel stack is the efficiency of collecting the Č photons emitted in the stack and focusing them on the PM photocathode. The Č light emission yield is 21 photons per 1 cm of aerogel in average and they are emitted at the angle of 14° with respect to the crossing charged particle direction. A special test box was designed and constructed - see Fig.6. The Č photons were reflected by the high quality mirror onto 2 Fresnel lenses which have focused them on PM photo-cathode. With this set-up the collection and focusing efficiency during the tests was found to reach 40 %.

However, since the working conditions in the HERA tunnel will be different from those at the test beam one should treat this result with caution - it is probably over-optimistic. In reality, the flux of bremsstrahlung photons falling on the face of calorimeter has a lateral spread of ≤ 5 cm. To simulate this during the tests one would have to move the axis of the test beam along x direction (horizonthaly) over the same distance. This is intended during the next tests.

If in front of the aerogel stack one places an absorber, the signal in aerogel increases proportionally to the number of charged particles leaving the absorber. The average number of detected photo-electrons (N_{pe}) are given in Table 6 together with the expectations from the EGS4 simulation [11].

Thickness of absorber (Pb)	N_{pe} (test)	N_{pe} (MC)
$0X_0$	5.16	5.2
$1X_0$	13.8	16.3
$2X_0$	26.4	33.0

Table 6: The average number of photo-electrons detected in tests together with the MC expectations.

Taking into account all the uncertainties in the MC simulation the agreement is fair.

The ADC distribution measured during the tests of aerogel is compared with that predicted by EGS4 MC in Fig.7 - the hatched histogram is the MC prediction. The low ADC enlarged tail is shown at the bottom of this figure. The agreement of measured and predicted ADC distributions is fairly good.

However, all the results quoted in this section should be considered as a very preliminary and one should wait for their confirmation during the forthcoming tests at the DESY test beam. During these tests the new large diameter PM will be used (see footnote on p. 13) and additional checks will be made like: dependence of the signal in aerogel on the test beam hit position, the optimalization of the test box construction and of the aerogel stacks thickness.

2.2 MC simulation of the active filter

The correlation between the number of photo-electrons and the corresponding read-out ADC's and energy detected in the calorimeter were studied with the help of Geant MC. The results are shown for the two generated energies of bremsstrahlung photons: 5 GeV (Fig.8) and 20 GeV (Fig. 9), in each figure separately for both aerogel stacks.

The interpretation of these plots is straightforward:

- the read-out ADC from aerogel is proportional to the number of photo-electrons (c, d);
- both, (a, b) the number of photo-electrons and the ADC value (e, f) are anticorrelated with the energy deposit detected in the calorimeter.

This study indicates that the aerogel-carbon active filter can be used as a tool to estimate the energy lost by a photon inside the filter.

Since the essential role in our design is played by the active aerogel-carbon filter it is desirable to compare the results of simulations of its performance by the two independent MC's. The comparison was made for several energies of the generated bremsstrahlung photons by EGS4 and Geant MC's and in Fig.10 we show it for 5 GeV photon and in Fig.11 for 20 GeV photon.

The comparison is made of the distributions of the number of observed photo-electrons detected in the first and second aerogel stacks. In the lower row histograms the predictions of the two MC's are overlayed. The overall agreement is fair.

2.3 Non-interacting photons

The results presented in this subsection are based on the Geant MC simulation of the aerogel-carbon active filter.

In Fig.12 and 13 the distributions of the photo-electrons, the corresponding ADC's in both aerogel stacks and the energy deposit in the calorimeter are shown for initial (generated) bremsstrahlung photon of 3.5 GeV (Fig.12) and of 10 GeV (Fig.13).

In both, the distributions of the number of photo-electrons and the corresponding ADC's, the distinct peaks at 0 are observed. In both distributions the separation between the peaks and the tails of the signal is better for 10 GeV than 3.5 GeV. The bottom rows of distributions present the energy deposits observed in calorimeter for non-interacting photons (NI), tagged either by the absence of the photo-electrons in both aerogel stacks or by the ADC cut $-6 < ADC < 6$ channels. The abscissa of these distributions is rescaled by a factor of ~ 16.3 up to get the deposits in GeV. This factor for the non-interacting photons corresponds to the calibration constant.

Since in the MC we additionally know which photon did not interact indeed, the three ways of identifying non-interacting photons are available:

- the absence of photo-electrons produced in PMT's reading both aerogel stacks;
- the ADC's consistent with no signal from both aerogel stacks: $-6 < ADC < 6$ channels;
- the true (MC defined) non-interacting photons.

The comparison of the different approaches is shown in Fig.14. The calculation based on the tabulated absorption cross sections is shown by a solid curve. The agreement of all three approaches and calculation is quite good. In Fig.14c we show the efficiency and purity of the sample of non-interacting photons selected on the basis of the absence of the photo-electrons.

The efficiency is here defined as:

$$Eff = \frac{(N_{pe} = 0) \bigwedge NI_{true}}{NI_{true}}$$

and purity as:

$$Pur = \frac{(N_{pe} = 0) \bigwedge NI_{true}}{N_{pe} = 0}$$

where NI_{true} stands for the number of non-interacting photons found from MC simulation.

For $E_\gamma \geq 7$ GeV both come close to 100%.

The ratio of the generated photon energy to that observed in the calorimeter is shown in Fig.15a as a function of photon energy for non-interacting photons. The energy resolution deduced for sample of non-interacting photons is weakly energy dependent and close to $\sim 15\%/\sqrt{E}$ what is expected for the calorimeter without a filter, used in simulations - see Fig.15b.

However, one has to be aware that at the increased luminosities the multiple bremsstrahlung at the single bunch crossing becomes more probable. Indeed, as shown in previous section, at the highest expected luminosities one expects in average as much as 2.4 bremsstrahlung photons/bunch crossing. Assuming that the number of bremsstrahlung events/bcr follows the Poisson distribution and knowing their average one can calculate the probability of any number (n_γ) of bremsstrahlung photons/bcr. Convoluting this probability with the non-absorption one it is easy to estimate the effect of the " pile-up ". As said before it affects the measured rate of NI photons - always decreasing this rate.

In all these studies it is convenient to use the average number of bremsstrahlung photons/bcr $=< n_\gamma >$ as a natural parameter (it is proportional to the actual luminosity). Therefore in Fig.16a we show the MC simulated dependence of the fraction F_{NI} of the bcr's for which a non-interacting photon was observed as the function of $< n_\gamma >$. As seen, this dependence is not monotonic at higher values of $< n_\gamma >$ (higher luminosities).[2] Thus,

[2] In the limit of the very large $< n_\gamma >$, F_{NI} tends to 0 since there is always at least one photon interacting in the filter.

measuring of F_{NI} may be used to determine the value of $< n_\gamma >$ only at not too high luminosity ($< 4 \cdot 10^{+31}$ cm^{-2}s^{-1}). However, in any case the measured F_{NI} has to be corrected for the effects of pile-up, always reducing its value, before one can use F_{NI} for calculation of luminosity.

The correction factor C_F by which one has to multiply the measured rate $R_{meas}(5)$ with trigger energy 5 GeV to get the rate corrected for pile-up effects is shown in Fig 16 as a function of $R_{meas}(5)$ or the luminosity.

Again, this correction factor C_F can be estimated using the MC and is shown in Fig.16b as the function of $< n_\gamma >$.

In summary, for the not too high luminosity ($< 4 \cdot 10^{+31}$ cm^{-2}s^{-1}) measuring F_{NI} ($< n_\gamma >$) allows the determination of the actual luminosity.

For the higher luminosity the described procedure may yield only a very useful check of the other luminosity measurements.

One should stress here, that the perspectives opened by the possibility of detecting the photons non-interacting in the filter with the high statistics, require further detailed studies.

3 The proposed design of the upgraded luminosity monitor

Following our 10 years experience in measuring the luminosity in the ZEUS experiment we propose to use the sandwich lead-scintillator calorimeter as the main detector of the bremsstrahlung photons.

In order to screen this detector from the substantially increased flux of synchrotron photons as compared to the present situation (almost by a factor of 7) the $4X_0$ filter in front of calorimeter is needed.

Since, after the HERA collider upgrade in parallel with the increase of the flux of synchrotron radiation the rate of measured bremsstrahlung photons will increase proportionally to the delivered luminosity (see section 1.2), the scintillator in calorimeter will be exposed to a substantial dose of radiation.

The light yield of the new generation scintillators SCSN81T2 (product of Kurarey Co.Ltd. [12]) deteriorates with the increasing dose of irradiation reaching 80% at the dose of 1.5 Mrad with the tendency of saturating at higher doses.

The expected dose in the calorimeter is of the order of 1.1 Mrad/year.

As proven in the section 2, our filter must be of the active type, i.e. we anticipate measuring the energy lost in the filter by appriopreate construction of it. As described in the section 2 the filter will consist of interlayed blocks of active material (aerogel) and the absorber (carbon and aluminum) - see the previous section for arguments of this choice.

In the whole detection scheme the role of the bremsstrahlung photons the exit window is of importance also. The window is at the distance of 92.5 m, i.e. 14 m in front of the detector. Its thickness is of great importance. It should be thick enough to prevent burning it by the heat released by synchrotron radiation. At the same time it acts as a part of filter - but a very inconvenient one, because the products of the bremsstrahlung photons interacting in the window may pass by the active filter and a part of the photon energy will be lost from detection. This issue awaits still solution and a compromise has to be found.

Having in mind all the mentioned limitations, we propose that the upgraded monitor will consist of:

- the bremsstrahlung exit window (still to be discussed with the HERA people);
- the active aerogel-aluminum/carbon filter of $4X_0$ thickness;
- the sandwich lead-scintillator calorimeter $24X_0$ deep with the position detector inserted after $4X_0$.

The overview of the detectors is shown in Fig.19

Tentatively the active filter will consist of:

- $2X_0$ block of carbon absorber (18.0×18.0) cm^2;
- aerogel counter, consisting of 5 aerogel SP-30 (Matsushita) plates ($11.0 \times 11.0 \times 1.0$) cm^3;
- another block of $2X_0$ carbon absorber (18.0×18.0) cm^2 and followed by the second aerogel counter - the same as the first one.

The aerogel stacks will be read by a large diameter 14 dynods phototubes.[3]

The cooling of the filter block of carbon is still under discussion.

The sandwich lead-scintillator calorimeter will be built of:

- 48 ($0.5X_0$ lead/2mm SCSN81T2 scintillator) layers of dimension (20.0×20.0) cm^2 (8 layers are before position detector and 40 after);
- 2 WLS light guides read by two PMT (Hamamatsu R5330 or R4275-02) - see Fig.20;
- the position detector built of 16 vertical and 14 horizontal scintillator fingers (SCSN81T2) of dimensions ($15.0 \times 1.0 \times 0.3$) cm^3 and ($18.0 \times 1.0 \times 0.3$) cm^3, respectively, each finger read by the PMT Hamamatsu R5600V - see Fig.21[4]

[3]Electron Tubes Ltd, type 99218 - 14 dynods, diameter 130 mm, photocathode 110 mm.

[4]The proposed position detector is the copy of that already built by us in 1996 and being in use since couple of years [13].

All three components: active filter, calorimeter and position detector will have the on-line light and charge tests. The light tests (flushing the LED on the PM's photocathode) and charge tests (injecting a charge at the entrance of electronics channels) are synchronized with the HERA clock and can be done both during the data taking and in stand-alone mode.

They are and will be done during the empty bunches (no electrons and no protons). The light test checks the stability of PMT's with the accuracy of 0.4% and charge test checks the stability of electronic channel with accuracy of 0.2%.

Mechanical construction of the monitor

	Dead_line	Expected man_months
Calorimeter	$\leq$ Sept 2000	8
Design Construction Assembly and tests (DESY)	$\leq$ Dec 1999 $\leq$ May 2000 $\leq$ Sept 2000	
Active filter	$\leq$ Sept 2000	7
Design - prototype Final design Construction Assembly and tests	$\leq$ Dec 1999 $\leq$ Feb 2000 $\leq$ June 2000 $\leq$ Aug 2000	
Position detector	$\leq$ Sept 2000	8
Design Construction Assembly and tests	$\leq$ Feb 2000 $\leq$ June 2000 $\leq$ Sept 2000	
COMPLETED	$\leq$ Sept 2000	23

Table 7: Milestones of the construction of the detectors.

	Materials
Photon Calorimeter	8500 DM
Active Filter	12500 DM
Position Detector	14000 DM
SUM	35000 DM

Table 8: Cost of the Detectors.

4 Readout Electronics and DAQ system for the upgraded luminosity monitor

The implementation described here is designed to satisfy the requirements of the proposed detector, however the system has been designed to provide sufficient flexibility and scalability to allow other detector set-up to be used.

4.1 Read-out Electronics

The front-end electronics are placed in a rack located under the tunnel floor ca. 10m away from the detector in the direction of ZEUS. This location is shielded from radiation by the massive concrete blocks of the floor and the remaining dose is expected to be 0.25 Gy/yr. Digitized data is transmitted to the experiment's electronics rucksack using fiber optic of length ca. 190m. The shielded cable tray is also used by the HV and slow control cables of the detector.

Electron energy data from the proposed 6m Tagger will also be used in the luminosity monitor system as a veto, in the trigger, or for use in off-line calibration of the photon calorimeter using the beam energy constraint.

The block diagram of the read-out electronics is shown in Fig.22.

4.1.1 Photomultipliers

The increased rates anticipated after the HERA luminosity upgrade have lead to the choice of using PMs with small gains (6-8 stages). These are expected to draw 5-10 μA. Decrease of the gain of the PM by the factor of 5 will extend the lifetime also by the factor of 5 i.e. up to 1-3 years. The necessary replacements can be carried out during the planned monthly access.

Hamamatsu [14], [15] R5330 and R4275-02 PMs have been selected as candidates for use in the calorimeter. The 30 metal package photomultipliers R5600-03 from the present electron position detector at 35 m from IP will be used. The gain stability of the selected calorimeter PMs has been measured and found to be <1%. No decision has been made w.r.t. the PMs to be used in the active filter.

The photomultipliers ([16]) type 9823B and 9921B (Electron Tubes Ltd.) and XP4500B (Philips) have been selected as candidates for the use in the active filter. However the final decision will be made after the December '99 tests.

The calorimeter and active filter high voltage will be supplied by CAEN modules located in the rucksack and the position detector HV by a step-up voltage converters in the tunnel rack. Both these systems have been used successfully in the existing monitor.

4.1.2 Front-end electronics

The PM signals of the calorimeter, active filter (Energies) and the position detector (Positions) are fed into the front end electronics of the tunnel rack where they are shaped and amplified before digitization in FADCs. The design parameters of the front end are shown in Tables. 9 and 10.

gain	10 - 40 (selectable)
linearity	+/- 0.3 % integral (0 to -3V)
bandwidth	$\geq$ 170 MHz
rise time (10% to 90%)	$\leq$ 2 ns
output noise	$\leq$ 50 μV rms

Table 9: Preamplifier & shaper design parameters

	8 bits	12 bits
fullscale	120 pC	250 pC
maximum safe input signal	- 1.0 V	- 1.5 V
max input frequency	11 MHz	12 MHz
coupling	DC	DC
accuracy	$\leq$1%	$\leq$0.2%
linearity	$\leq$ 1%	$\leq$ 0.5 %
integration time	60 ns	55 - 60 ns
integrator reset time	30 ns	20 - 25 ns

Table 10: Integrators & FADC design parameters

The Position information requires 8 bit FADC resolution and will allow the reuse of the FADC system of the existing luminosity monitor's electron and photon position detectors, as well as the experiments 8m Tagger. The maximum sensitivity of a single positron detector channel to the single NIP signal is expected to be 12 pC.

The Energy information requires high speed integrators for nano-second pulses proceeding a 12 bit resolution FADC system. The design of the integrator is expected to require the most effort and the parameters are shown in Tab. 10. The maximum signal charge delivered by the PMs is expected to be 10pC.

4.1.3 Data link

A new data link will be implemented to transmit digitized Energy and Position data from the front end output buffers to the rucksack electronics. The existing system cannot be reused due to the increase in number of readout channels and maximum word length (8 to 12 bits). It is intended to use DataMover Gigabit Fibre Optic Links [17] from Broadband Communications Products, Inc. Each link has a nominal bandwidth of 1Gbit/s and is therefore capable of transmitting the required 80 bits of data within the 96ns time window defined by the bunch crossing rate of 10.4MHz. The preliminary design of the link drivers have been finalized and reliability and operation tests of a prototype are planned. Radiation hard [18] multi mode (50/125um) fiber with ST connectors will be used. The proposed design requires 4 links: 1 for the Energy data (6x12 bits) and 3 for the Position data (3x10x8 bits). Data from the 6m Tagger will require additional links of the same type.

4.2 DAQ System

4.2.1 Rucksack trigger and data handling electronics

The DAQ design foresees that all the link receiver, trigger and data handling electronics can be inserted into a single 9u VME custom backplane crate using. A schematic of the board functionality is shown in Fig. 23 and the slot allocation in Fig. 24.

The following boards must be designed and manufactured:

- A GFLT interface board interfaces the DAQ system to the experiments Global First Level Trigger [19]. The GFLT distributes, via twisted pair cable, all the synchronization and control signals (HERA clock, bunch number, etc.) required by the lumi DAQ when participating in a run. Necessary synchronization and control signals are then passed on to the front end and other crate boards.

- Energy, position and 6m Tagger data collection boards receive data from the front end and 6m Tagger data links and store the data in two circular buffers. Buffer 1 is a wrap round store containing the data of the last 220 events (bunch crossings). GFLT accepted events are read from this buffer by the CPU via VME and stored in local memory awaiting a GSLT trigger decision. Buffer 2 is latched and stores data from 64k bunch crossings and is readout when full. This data is readout by the CPU via VME and sent via IP/Fastethernet to an additional CPU, where online luminosity and other monitoring calculations are made. A fraction of the buffer 2 data is transfered to the experiments event builder as part of environmental events. The link receiver and buffers are a common feature of all the data collection boards. The Energy and 6m Tagger additionally pass some or all of the data received to the Calibrator or Luminosity processor boards. The VME crate has space for 1 Energy, 3 Position and up to 5 Tagger boards.

- The Calibrator board receives event energy data and corrects the raw data using calibration values determined off-line and down loaded into lookup tables. The resulting data is forwarded to the luminosity processor.

- The Luminosity processor board will transmit the energy sum, evaluated from the Energy inputs to the Calibrator, to the GFLT where it can be used to evaluate the GFLT trigger decision. Additionally the board increments "on-line" scalars (number of Bremstrahlungs, empty bunch Bremstrahlungs, active time, etc) which are readout, via VME, and used to calculate the on-line luminosity. A further set of scalars, "off-line", are similarly evaluated and provide per bunch information which is used off-line with event samples from the 64k buffers during the calculation of the final luminosity.

Available third party boards used are:

- The NIKHEF 2TP is used to send the GSLT accepted data to the EVB (Fig.25). This data is transfered by the PowerPC CPU from data in local memory to the 2TP triple port memory (TPM) via the VMEbus. The EVB side TP of the 2TP, which is booted by the EVB TP network, then forwards the TPM event data to the Third Level Trigger (TLT) processor farm.
- The Motorola PowerPC MVME 2700 (or later upgrade) runs DAQ software which carries out any necessary actions required to prepare for take data during data taking. During data taking the CPU is required to readout data collector memory buffers, as described above, and handle actions required by the GSLT and EVB interfaces. Note that the detector participates in the experiment's GSLT trigger decision by transmitting some energy sum data to the GSLT. It is proposed to use a PC-PCI board transputer interface board connected to the CPUs PMC slot. The LynxOS operating system has been chosen.
- The HERA MDM boards are provided by HERA and allow the electron and proton bunch currents to be read.
- The Crate controller board allows the crate temperature, voltages and currents to be monitored, via GPIB bus, and may be used to generate VMEbus resets and turn the crate on/off.

4.2.2 Slow Control

The slow control of the DAQ system is required for:

- moving the calorimeter, filter and lead absorbers from their safe, shielded, position to their data taking positions,
- enabling and disabling the light and charge calibration and data transmission test system,
- controlling the HV system, and
- temperature measurement.

These functions will be realized by a control board installed in the tunnel rack. Communication between the board and it's controller, in the electronics crate, is provided by an RS485 serial connection.

Note that major parts of the slow control system are already used in the existing monitor.

4.2.3 DAQ Software

As mentioned above the 9U electronic crate CPU fields all the interrupt driven VME transfers between boards and the GSLT and EVB data requirements.

A second CPU, in the 6U service crate, receives monitoring information, via a dedicated Fastethernet connection, and is required to run performance monitoring software (online luminosity calculation, shiftcrew luminosity display, generate histograms, data quality monitoring, etc.) and export the results to the experiment and the HERA control room. The machine also hosts the connections to the experiments central run and slow control systems and uses the electronics crate CPU as a slave to carry out the actions required. An extensive re-write of existing software and some additional programming effort is required.

4.2.4 Calibration and test system

Photomultiplier and analogue front end electronics performance will be monitored using LED light pulses, injected into the lightguides of all PMs, and charge injection into the pre-amplifier inputs. The correct transmission of digital data through the data links and subsequent electronics will be tested by inserting known bit patterns into the link transmission cards.

All the tests described will be made during data taking by triggering a given test on the occurance of a chosen empty electron bunch.

4.2.5 DAQ data handling performance

The performance required by the electronics from the front end to the custom cards of the 9U VME crate is determined entirely by the HERA bunch crossing rate of 10.4MHz (96ns). Thereafter the performance is a function of the GFLT and GSLT trigger rates which are determined by the design and performance of the ZEUS trigger and data flow system.

The data handling requirements of the electronics crate components are driven by the VMEbus data access, GFLT and GSLT rates (Fig.25). On GFLT trigger accept 100B of Energy (10B), Position (30B), 6m (assumed to be 60B) and trigger data (4B) is transferred from the collection board wrap buffers to readout CPU local memory. On GSLT accept this data is then moved to the EVB 2TP TPM buffer. Additional loading results from data transferred for inclusion in the environmental triggers (estimated to be 4kB/s) and the monitoring requirements of the service CPU (8kB/s).

Assuming a maximum GFLT rate of 1kHz, a GSLT rate of 100Hz (which is likely to be a conservative estimation) the total VMEbus load is calculated to be 120kB/s. This is small compared to the programmed, non DMA, I/O rate of 4MB/s and no significant loading problems are anticipated.

The GSLT requires that detector data intended for use in the GSLT trigger be available within 3ms of the GFLT accept trigger for the event and the EVB requires that its data be available within 50ms. These requirements should be easily satisfied by the proposed system. Note that the GFLT and GSLT accept interrupts which drive the data transfers will be prioritorized.

4.3 Milestones and cost estimation

	Dead line	Expected man_months
front end electronics	$\leq$ Oct. 2000	7
prototype of optical transmission	$\leq$ Dec. 1999	2
installed optical transmission system	$\leq$ July 2000	5
prototype of the integrator and FADC	$\leq$ Dec. 2000	12
slow control	$\leq$ June 2000	2
step motors	$\leq$ Dec. 2000	2
tunnel installation work	$\leq$ Nov. 2000	3
tunnel mechanical work	$\leq$ Oct. 2000	3
DAQ boards	$\leq$ Dec. 2000	15
software: prototype of GSLT and EVB connection	$\leq$ Mar. 2000	6
software: test of the new hardware readout	$\leq$ Dec. 2000	8
software: system complete	$\leq$ Feb. 2001	9
COMPLETED	$\leq$ Feb. 2001	74

Table 11: Milestones of read-out electronics and DAQ

	Materials
photomultipliers	15000 DM
front-end	6000 DM
integrators and FADC's	15000 DMM
optical transmission links	30000 DM
crates	30000 DM
step motors	10000 DM
DAQ board + design software	20000 DM
slow control board	1000 DM
SUM	127000 DM

Table 12: Cost of the readout system.

CPU– PowerPC MVME2700 – two boards	2 * 8000 DM
Hard drive (9GB)– two pieces	2 * 1100 DM
VME Crate	10000 DM
PMC-Dual100BT-FP	2 * 1100 DM
PCI – transputer link interface	4500 DM
PC-Caddy (passive VME-bus carrier for 2 PMC modules)	2600 DM
SUM	37500 DM

Table 13: Cost of related CPU systems

5 MC simulation of the proposed luminosity monitor

The performance of the described in the previous section new luminosity monitor was simulated both by Geant and EGS4 MC's [23].

In order to correct for the energy lost in the filter we use the information from the active filter. The simple formula correlating the information from the active filter with that from the calorimeter is:

$$E_{corr} = a_1 \cdot A_1 + a_2 \cdot A_2 + b \cdot E_{Dcal} \tag{1}$$

where A_1 (A_2) is the number of photo-electrons or properly normalized ADC read-out from the first (second) stack of aerogel and E_{Dcal} is the energy deposit in the calorimeter.

In Fig.26 we show the coefficients a_1, a_2 and b obtained from the fit of observed deposits of energy in the filter and the calorimeter for bremsstrahlung photons of fixed energy. As a measure of the deposit the number of photo-electrons was used (see section 2.2).

To see the values of A_1, A_2 in terms of number of photoelectrons ($N_{pe1,2}$) see Fig.10 and 11. Eg. for 5 GeV photons the averages of these numbers are $\sim 40-50$ for A_1 and $\sim 60-70$ for A_2.

The comparison of the results obtained with the two discussed MC's is shown in Fig.26, where the parameters a_1, a_2 and b and the energy resolution for corrected and uncorrected energy deposits are shown as the function of generated photon energy. Despite some disagreements between MC's in some cases (i.e. parameter b is different by 3% and the uncorrected energy resolution by 6%) the overall agreement is satisfactory.

The incoming photon energy can be estimated using the information from the calorimeter and active filter (E_{corr}) or only calorimeter (E_{Dcal}). The distributions of E_{corr} and E_{Dcal} are shown in Fig.27 for 5 GeV photons and in Fig.28 for 20 GeV photons and were simulated by Geant MC. The same distributions obtained from EGS4 simulations are shown in Fig.29 and 30. Upper plots (a) show the corrected energy distributions obtained by fit of the formula (1) to the observed distributions and the lower plots (b) show the uncorrected calorimeter energy distributions. In each plot the deduced energy resolution is quoted.

The most important conclusions are:

- the fit parameters a_1, a_2 and b are weakly energy dependent;
- the correction of the observed in the calorimeter energy exploiting the information from the active filter improves the energy resolution from $\sim 90\%/\sqrt{E}$ to $\sim 25\%/\sqrt{E}$.

The MC study of the longitudinal distribution of the radiation dose shows (Fig.17) that a scintillator close to the maximum of the cascade (at the depth of $\sim 5X_0$) would receive a dangerous dose (twice or more that of average). The radiation damage of these scintillators would certainly lead to the decrease of light output and energy deposit in the calorimeter but it could also introduce non linearity in the energy measurement. We have studied these effects using Geant MC. The results are shown in Fig. 18.

The decrease of light output has to be corrected by adjusting either the calibration constant or the PMT's gain. However even for large damage (~ 20 %) the deviation from linearity does not exceed 1%.

An independent estimation of the rediation damage of the scintillators is based on the up to now experience of running of our sandwich lead/scintillator calorimeter. The scintillator type SCSN38 is used in our present calorimeter and photon position detector. After ~ 3 years running the scintillator fingers in the position detector got destroyed beyond the level of further acceptance.[5] Since the new generation scintillator SCSN81T2 resistevity to the irradiation is about 2 - 3 times better than that of SCSN38 we estimate that the new scintillator irradiated to $\sim 150\ pb^{-1}/yr$ can stand it with the same loss of efficiency. Therefore on would face changing the scintillators once per year.

The construction of the calorimeter is such, that the exchange of the individual scintillator layers will be easy. The identification of the scintillator which should be exchanged will be done with the help of the Co^{60} source movable along both sides of the calorimeter. The scintillator response to the irradiation by this source can be controlled and its destruction judged in a time dependent way.

6 Calibration and acceptance of calorimeter

Since our calorimeter is situated behind a thick filter, the proper calibration and detailed knowledge of the energy scale involved is of primary importance. To make such calibration realistic one should test the whole set-up i.e. the calorimeter with the inserted position detector and the filters. One should make the calibration at the test beam, however the calibration may change in time and one needs the checks which can be repeated and made during the run.

Several checks can be done using the HERA beams and the planned electron tagger at 6m from the I.P. [22]

- The fit of the observed response distribution by the realistic MC determines the calibration constant. The cross check of this determination is the calculation of the calibration constant from the end point of response distribution.

[5]The destruction is judged by the deterioration of the light output from the fingers of the position detector which after $\sim 50\ pb^{-1}$ lost about 25% of their light yield.

- The above method is particulary reliable for the photons non-interacting in the filter (no signals from aerogel).
- The electron tagger at 6 m from the IP is expected to have 100% acceptance for the electron energies in the interval 6 to 9 GeV with 27.5 GeV electron colliding beam energy and in the interval 2.6 - 3.9 GeV with 12 GeV electron injection energy. These intervals correspond ($E_\gamma + E_e = E_e^{beam}$) to the photon energies in the interval 18 - 21 GeV and 23.6 - 24.9 GeV respectively. Since the energy resolution of the tagger is very good ($\sim 15\%\sqrt{E}$) the energy of these photons is relatively well known and will be used in testing the calibration of the photon calorimeter.
- The accuracy of calibration using described above tagged electrons improves if one selects the photons non-interacting in the filter. In this last case the photons measurement by calorimeter tests the calibration of the tagger.

The acceptance of calorimeter is purely geometrical and it was estimated with the help of MC [4, 5] to be for electron beam (92 - 95)% and for positrons (94 - 96)% depending on the beam tilt.

7 Calculation of luminosity

The luminosity L is defined by the relation

$$R = L\sigma \tag{2}$$

where R is the rate of the process with the cross section σ. Therefore to determine L from rates of bremstrahlung photons selected by various cuts one has to calculate the fractions of bremstrahlung cross section σ_{obs} corresponding to these cuts and to the geometrical acceptance of the detector, as well as to correct the rates for possible various contaminations.

The problem of rates will be discussed in section 6.4.

The calculation of σ_{obs} requires knowledge of the theoretical cross section, the response of the calorimeter and its geometrical acceptance. The uncertainties of these factors result in the systematic error of σ_{obs}. Here, we concentrate on the possible error coming from the uncertainty of the calorimeter response.

Neglecting the geometrical acceptance, for a realistic calorimeter without filter, σ_{obs} can be obtained by integrating Bethe Heitler formula in an energy range used for photon selection. For a calorimeter with a response proportional to the incident photon energy and gaussian smearing $\Delta E/E \leq 0.25/\%\sqrt{E}$ a correction due to the finite resolution is small. The difference in σ_{obs} calculated from Bethe-Heitler distribution and from convolution of Bethe-Heitler distribution with quoted gaussian energy smearing is of the order of 0.1%. The calibration constant c_γ which translates ADC counts to energy, depends on the electronics and it has to be determined for each run. This calibration is done by fitting $e-gas$ bremsstrahlung spectra [6] for electron pilot bunches. The uncertainty of c_γ

[6] $e-gas$ spectra are free from the beam size problem and have reduced pile-up effects.

is about 0.5 % which reflects in the error of σ_{obs} up to 0.3% depending on the selection of photon energies.

The uncertainty of the theoretical cross section is about 0.4%, mainly due to the beam size effect, so together with the best possible knowledge of the detector response, the minimum systematic error on the luminosity value is 0.5%.

The nessessity of shielding the calorimeter with $4X_0$ filter (see sec 1.1) causes that such a good photon energy measurement cannot be performed in reality. The energy spectrum observed in the calorimeter is considerably distorted by the energy loss in the filter, however this energy loss can be estimated using the information from the active filter. Therefore, to measure the luminosity with the proposed upgraded monitor one can do it using either:

- the directly measured calorimeter energy (method 1), or
- the calorimeter energy corrected using the information from the active filter (method 2), or
- the selection of photons non-interacting in the filter and the calorimeter energy (method 3).

7.1 The photon selection based on the calorimeter energy (method 1)

The calorimeter energy spectrum is

$$\sigma_{obs}(E'_{cal}) = \int_{E_{min}}^{E_{beam}-m_e} dE_\gamma \sigma(E_\gamma) * P(E'_{cal}, E_\gamma) \tag{3}$$

where $P(E'_{cal}, E_\gamma)$ (calorimeter response function) is the probability that for a photon incident energy E_γ the calorimeter response energy is E'_{cal} where $E'_{cal} = k \cdot E_{cal}$ and k is the scale adjustment constant.

In order to calculate σ_{obs} one must know the calorimeter response function P(E'_{cal}, E_γ). Without the real data P(E'_{cal}, E_γ) can be only studied with the help of MC. In Fig.31 we show the calorimeter response function (points with errors) for generated different initial energies E_γ. This function has two maxima. It turns out that the sum of two weighted Weilbull distributions [24] of the general form:

$$\frac{c}{\alpha}(\frac{x-x_0}{\alpha})^{c-1} * e^{-(\frac{x-x_0}{\alpha})^c}$$

fits the obtained E'_{cal} distributions at all considered energies with the two sets of energy dependent parameters c, x_0 and α (see full curves in Fig.31). The parameters can be expressed as the simple functions of energy.

The first to maximum corresponds to the photons which interacted in the filter and lost some energy and its position is at:

$$(E_{cal})_{max} = x_0 + \alpha \cdot (\frac{(c-1)}{c})^{\frac{1}{c}}$$

The second maximum is due to the non-interacting photons and is at $E'_{cal} = E_\gamma$.

To test the reliability of this approach the full spectrum of $e - gas$ bremstrahlung photons was simulated and fitted using the parametrized form of $P(E'_{cal}, E_\gamma)$ with two free parameters: scale adjustment constant and the position of the first maximum. The simulated and the fitted spectra are shown in Fig.32 (χ^2/ndf is 1.3). By changing these two parameters one can estimate the systematic errors in this method and this exercise leads to the following conclusions:

- the scale constant can be determined with an 0.5% error;
- the fitting procedure is sensitive to the position of the first maximum. The uncertainty of the position of the first maximum of 0.5% introduces the systematic error of σ_{obs} between 0.8% to 1.5% depending on selected energy range.

With this method the contribution to the luminosity error from the calorimeter response does not exceed 2.5%.

7.2 The photon selection based on the corrected energy (method 2)

The photon energy can be reconstructed as weighted sum of the calorimeter and active filter ADC counts (see formula 1). The parameters a_1, a_2, b (formula 1, Fig. 21) used in calculation of E_{corr} are weakly energy dependent. In practice if one keeps a_1, a_2, b constant one should compensate for their energy dependence: E_γ as

$$E_{corr} = E_\gamma + c_{nl} * E_\gamma^2 + c_{shift} \tag{4}$$

where the constants c_{nl} and c_{shift} are very small. The resulting resolution comes up to be good - $\Delta E/E = 0.25\%/\sqrt{E}$. The summation (in formula 1) can be done on-line, therefore it is possible to select photons by cuts on their corrected and nearly true energy. The expected values of c_{nl}, c_{shift} and the resolution are similar to those of the detector used in 1996 (with $2X_0$ filter) [20]. They can be found from the fits of the experimentally observed $e - gas$ spectra with similar precision. The systematic error on σ_{obs} due to the uncertainty of the calorimeter response does not exceed 0.5%.

7.3 The selection of photons non-interacting in the filter (method 3)

As it was shown before, using the active filter working in a veto mode, such selection can be done with high efficiency for photon energies greater then 7GeV. For this subsample

$$\sigma_{obs}(E_{cal}) = \int_{E_{min}}^{E_{beam}-m_e} dE_\gamma \sigma(E_\gamma) * P(E_{cal}, E_\gamma) * A(E_\gamma) \tag{5}$$

where $P(E_{cal}, E_\gamma)$ is now gaussian distribution with $\Delta E/E = 0.15\%/\sqrt{E}$ and $A(E_\gamma)$ is the probability that a photon passes through the filter without an interaction.

$A(E_\gamma)$ is weekly decreasing function of energy (see Fig 15a). Since, in this case the photon energy is directly measured by the calorimeter the error of σ_{obs} due to the uncertainty of the calorimeter response is negligible. The dominating contribution to the systematic error comes from $A(E_\gamma)$. It depends on the size and density of the filter and is estimated to be below 1%.

7.4 Pile-up effects

As discussed in section 1.2 the increasing probablility of the multiple bremsstrahlung events in a single bcr, with the increasing luminosity (so called pile-up effects) leads to the severe problems in the luminosity determination. The pile-up effects affect the counting rate.

The ratio of the true bremsstrahlung rate (including the multiple counts for the multiple events/bcr) to the measured one as a function of the measured rate was simulated using the MC.

- It is shown in Fig.33 for the method 1 of the selection of bremsstrahlung photons (section 6.1) using the different energy threshold triggers. Looking at the energy trigger of $E_\gamma \sim 7$ GeV, which is the least biased from the pile-up effects (Fig.5) even at the highest rates corresponding to the highest expected luminosity, the deviation of this ratio from 1 does not exceed ~ 2 %.

  Using Fig.33 one can correct measured rates for different energy triggers. The comparison of luminosities obtained for various triggers allows the reduction of the error on luminosity due to the pile-up effects to 0.5%.

- Similarly, in the case of using the corrected energy of the photon (method 3) the estimated error due to the same pile-up effects is ~ 0.5 %.

- In the case of non-interacting photons, the error due to the pile-up effects has two major components:

  - the error on the aerogel counter efficiency due mainly to our non precise knowledge of the aerogel and filter properties ($\sim 1\%$).
  - and the error on $< n_\gamma >$/bcr estimation.

  The latter is related to the accuracy of the theoretical cross section calculation at low photon energies (due to the beam size effect). It is estimated to be ~ 1.5 %.

  Thus the total error an the rate of NI photons, due to the pile-up effects is ~ 1.8 %.

7.5 Conclusions

With the help of the proposed monitor one can measure the luminosity on- and off-line exploiting the three independent methods of the bremsstrahlung photons selection.

The main contributions to the total error on the luminosity value determination, estimated on the basis of the MC simulations are summarized in Table 14.

Method	Uncertainty of the calorimeter response	Pile-up effects	Other contributions *	Total
Directly measured calorimeter energy	$\leq 1.5\%$	$\sim 0.5\%$	1%	$\leq 1.9\%$
Calorimeter energy for non-interacting photons**	$\sim 1\%$	1.8%	1%	~2.3%
Calorimeter energy corrected for the loss in the filter	$\sim 0.5\%$	0.5%	1%	~1.2%

Table 14: The errors on the off-line determined luminosity based on the MC simulations. *) Include the uncertainty of: the theoretical cross section, the geometrical acceptance, the contamination from other than bremsstrahlung processes.**) This method works for luminosity $< 4 \cdot 10^{31}$ cm^{2}s^{-1}

Finally, it is needless to stress that the independent measurement of the energy of brem - sstrahlung photon, even in the limitted energy interval, would be of great importance for the control of the calorimeter energy measurement. Such measurement could be done with the 6m electron tagger.

At the same time it would be desirable to control the overall normalization in our luminosity measurement by an entirely independent luminosity measurement, based e.g. on the detection of QED Compton effect.

8 Manpower and cost estimation

The team involved in the realization of the project consists of:

- 10 physicists;
- 1 system programmer;
- 3 analogue and 3 digital electric engineers;
- 1 mechanics engineer;
- 3 technicians.

The involvement of each of these persons will be at the level of (50 - 100) %.

Total expected cost

Materials	162000 DM
Man_power	97 man_months

References

[1] D. Kisielewska et al., "Fast Luminosity Monitoring at HERA ", DESY-HERA Report 85-25

[2] The ZEUS Detector, Status Report 1993

[3] J. Andruszków et al., " First Measurement of HERA Luminosity by ZEUS Lumi Monitor ", DESY 92-066, May 1992

[4] L.Suszycki - private communication; ZEUS Note in preparation

[5] L.Suszycki - private communication; ZEUS Note in preparation

[6] U.Schneekloth, " The HERA Luminosity Upgrade ", DESY HERA 98-05, 1998

[7] S.K. Sahu et al., " Measurement of Radiation Damage on Silica Aerogel Cerencov Radiator ", KEK Preprint 96-4, BELLE Preprint 96-1, NIM A 382 (1996) 441

[8] K. Olkiewicz, A. Eskreys, " Off-line Luminosity Calculation in the ZEUS Experiment in 1997, 1998 and 1999 ", ZEUS Note 99-044

[9] K. Piotrzkowski " Observation of the beam-size effect at HERA ", Z. Phys. C67 (1995) 577

[10] Matsushita Electric Works, Ltd, Osaka, Japan,
R. De Leo et al., NIM A401 (1997) 187
P. Carter, B. Filippone, " Caltech Studies of Hermes Rich Aerogel ", Feb. 1998, Draft
R. De Leo et al., "Optical characterization of n=1.03 silica aerogel from Matsushita "

[11] J. Figiel, A. Kotarba - private communication; ZEUS Note in preparation

[12] T. Hasegawa et al., NIM A311 (1992) 498

[13] A. Eskreys, Report on the ZEUS meeting, Bristol 2-5 April, Proc. Vol II, p. 201 (1997)

[14] Hamamatsu Photonics K.K. Tube Center, "Photomultiplier Tubes and Assemblies for Scintillation Counting & High Energy Physics"

[15] Hamamatsu Photonics K.K. Electron Tube Center 1994, Cat. No.TOTH9001E01 , "Photomultiplier Tubes principle to application"

[16] Electron Tubes Ltd., " Phototubes and Accessories " catalogue 150 9001.

[17] Broadband Communications Products, Inc. "Data sheets"

[18] Fujikura Ltd. October 30, 1991, No. BB-16304A, "Specification Radiation Resistant Step Index Multimode Optical Fiber"

[19] K.Tokushuku, ZEUS Note. 88-098, "GFLT Design Document I - interface to component"

[20] J. Andruszków et al., " Luminosity Measurement in the ZEUS Experiment ", ZEUS note in preparation, will be submitted to NIM A

[21] K. Piotrzkowski, L. Suszycki, " BREMGE, a Monte Carlo Generator of High Energy Electron-Proton and Electron-Nulceas Bremsstrahlung Events ", Proc. of the Workshop, Physics at HERA, Oct. 1991, p.1463, Hamburg

[22] R. Graciani " A new Electron Tagger for ZEUS ", ZEUS-Note 99-067

[23] A. Kowal private communication; ZEUS Note in preparation

[24] N.L. Johnson, S. Kotz " Continuous univariate distributions - 1 ", Houghton Mifflin Company - Boston (1970), p. 250.

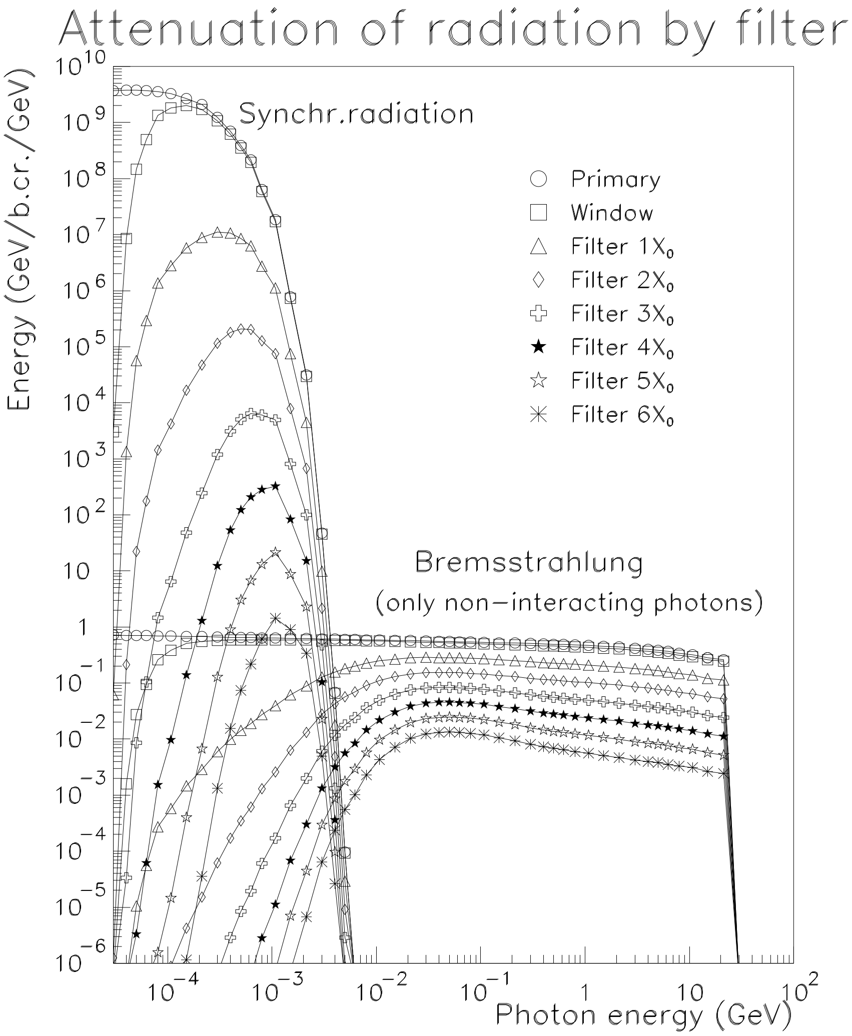

Figure 1: Attenuation of the synchrotron radiation and bremsstrahlung photons by carbon filters of variable thickness.

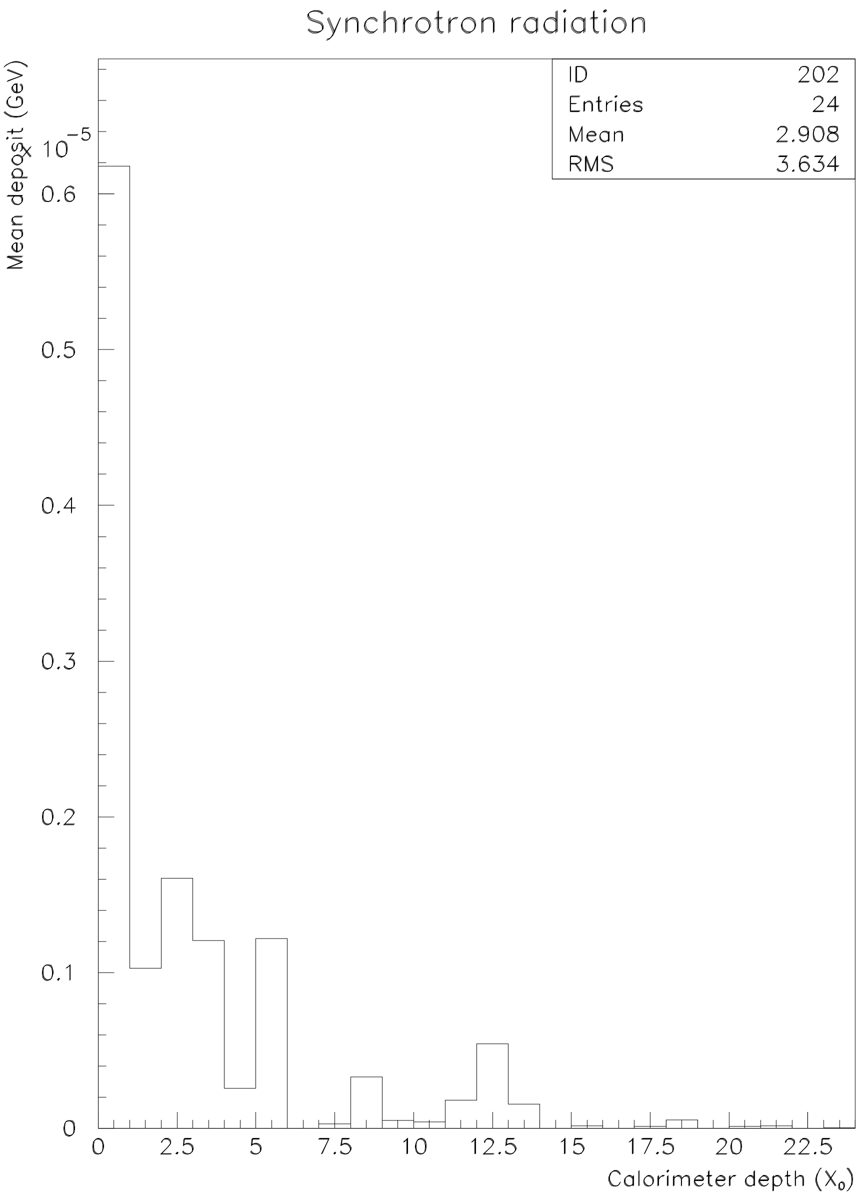

Figure 2: Synchrotron radiation deposits in the calorimeter scintillators.

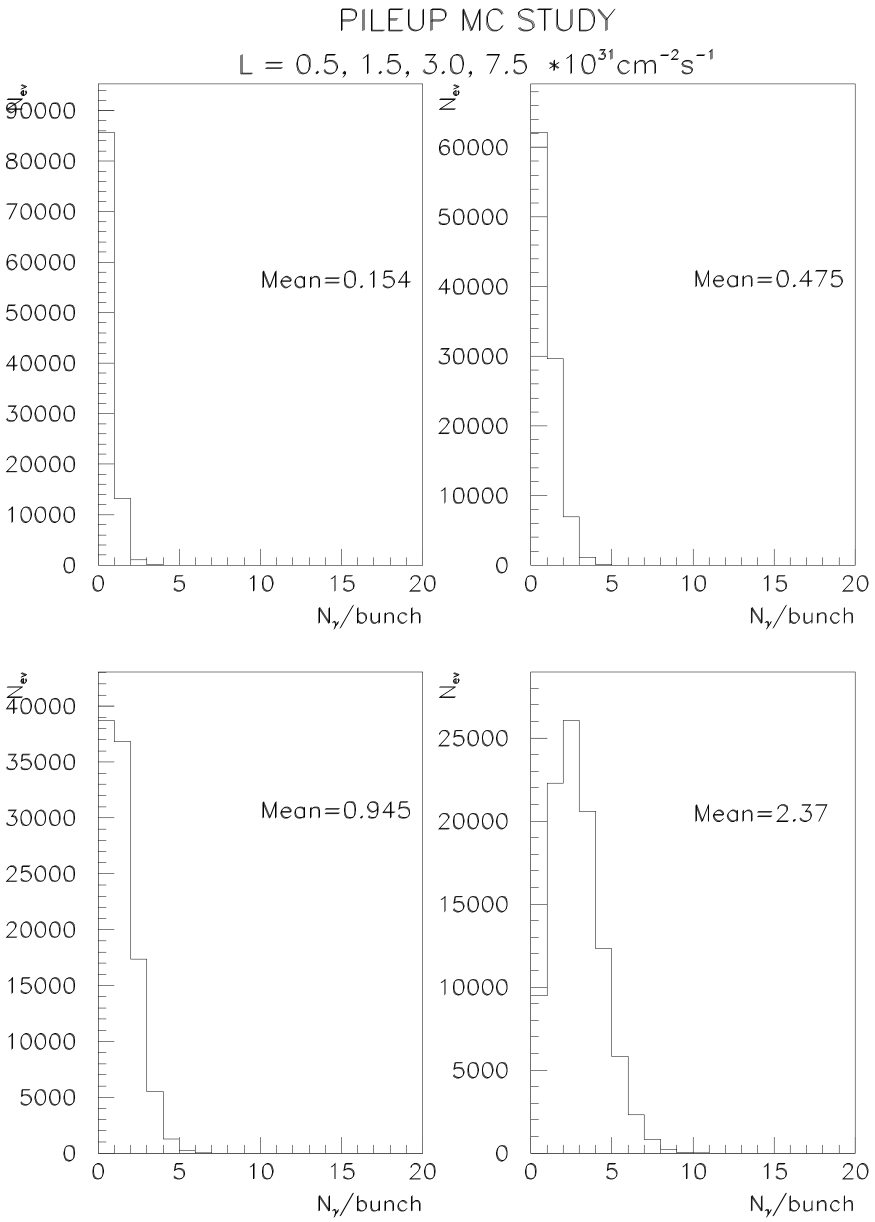

Figure 3: The multiplicity of bremsstrahlung events in a single bcr for 4 values of luminosity.

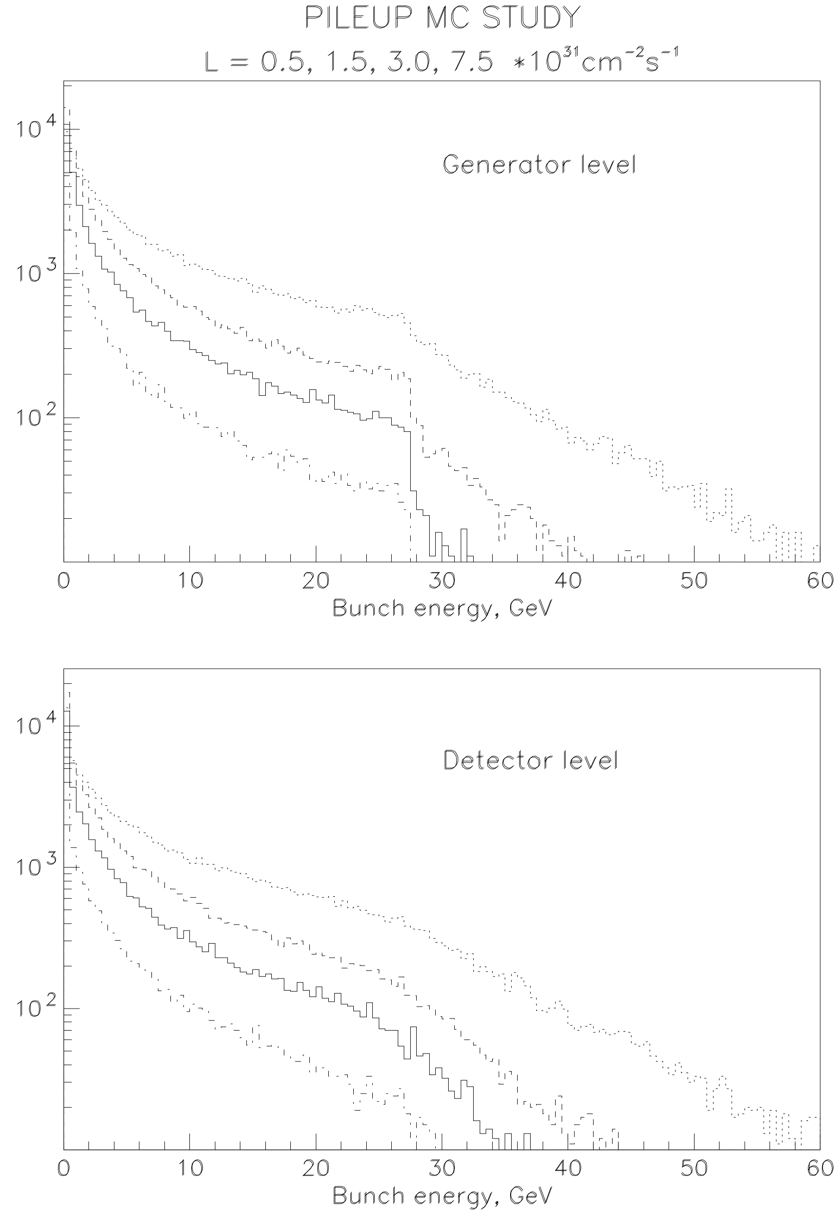

Figure 4: The expected energy spectra as observed in the calorimeter for 4 values of luminosity, at the generator and detector level. $L = 0.5 \cdot 10^{31}$ cm^{-2}s^{-1} - dashed-dotted curve, $L = 1.5{\cdot}10^{31}$ cm^{-2}s^{-1} - full curve, $L = 3.0{\cdot}10^{31}$ cm^{-2}s^{-1} - dashed curve, $L = 7.5{\cdot}10^{31}$ cm^{-2}s^{-1} - dotted curve.

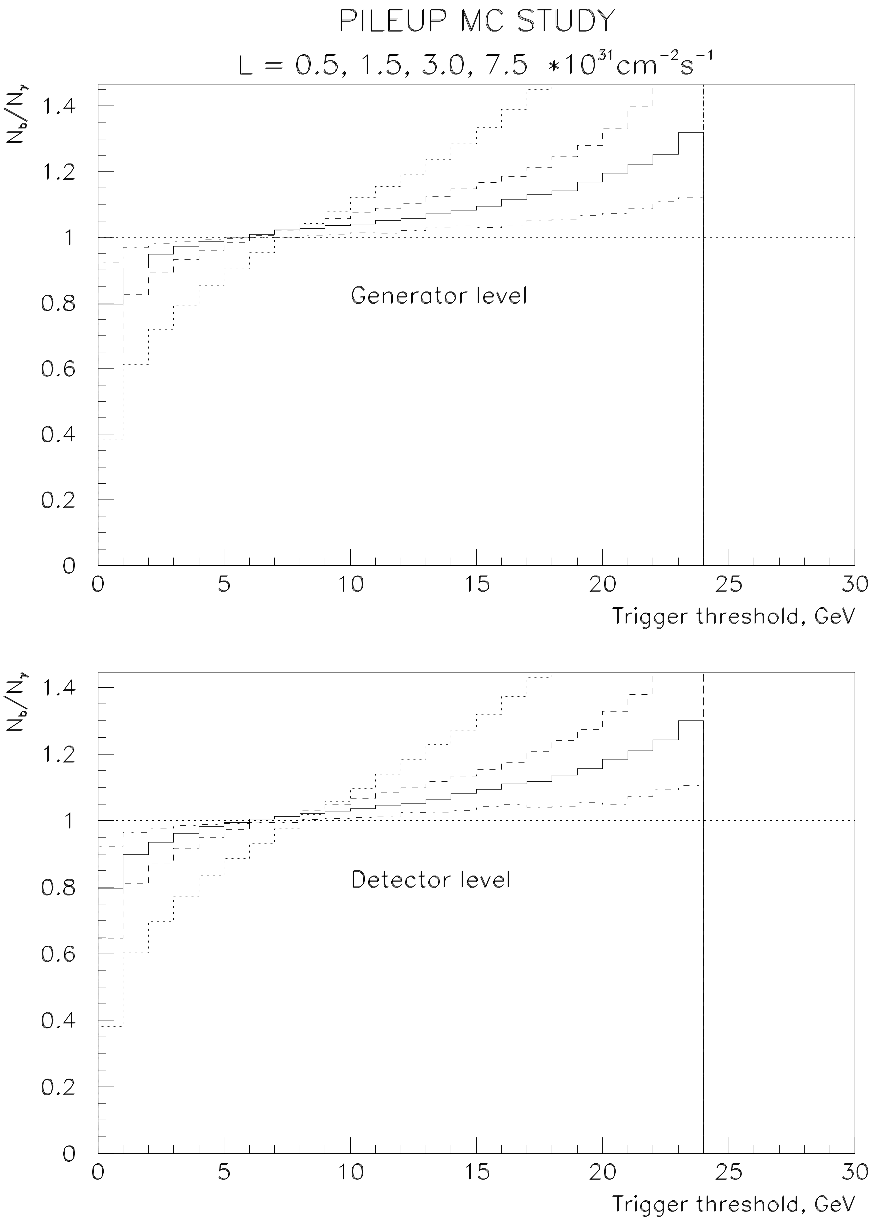

Figure 5: Pile-up effect as a function of the threshold trigger, for different luminosities. See Fig.4 for explanation of curves.

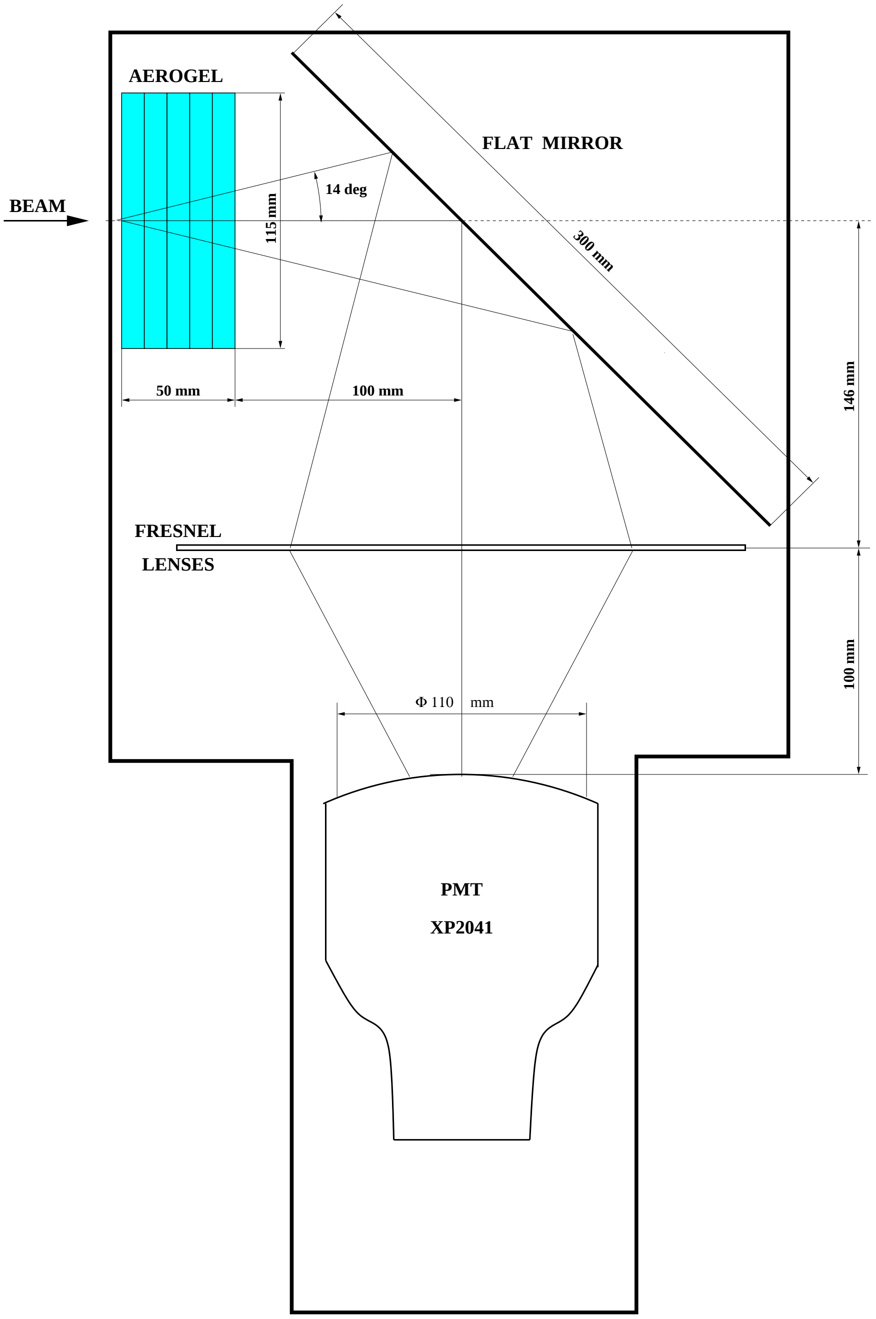

Figure 6: Prototype of the test aerogel Cerenkov detector.

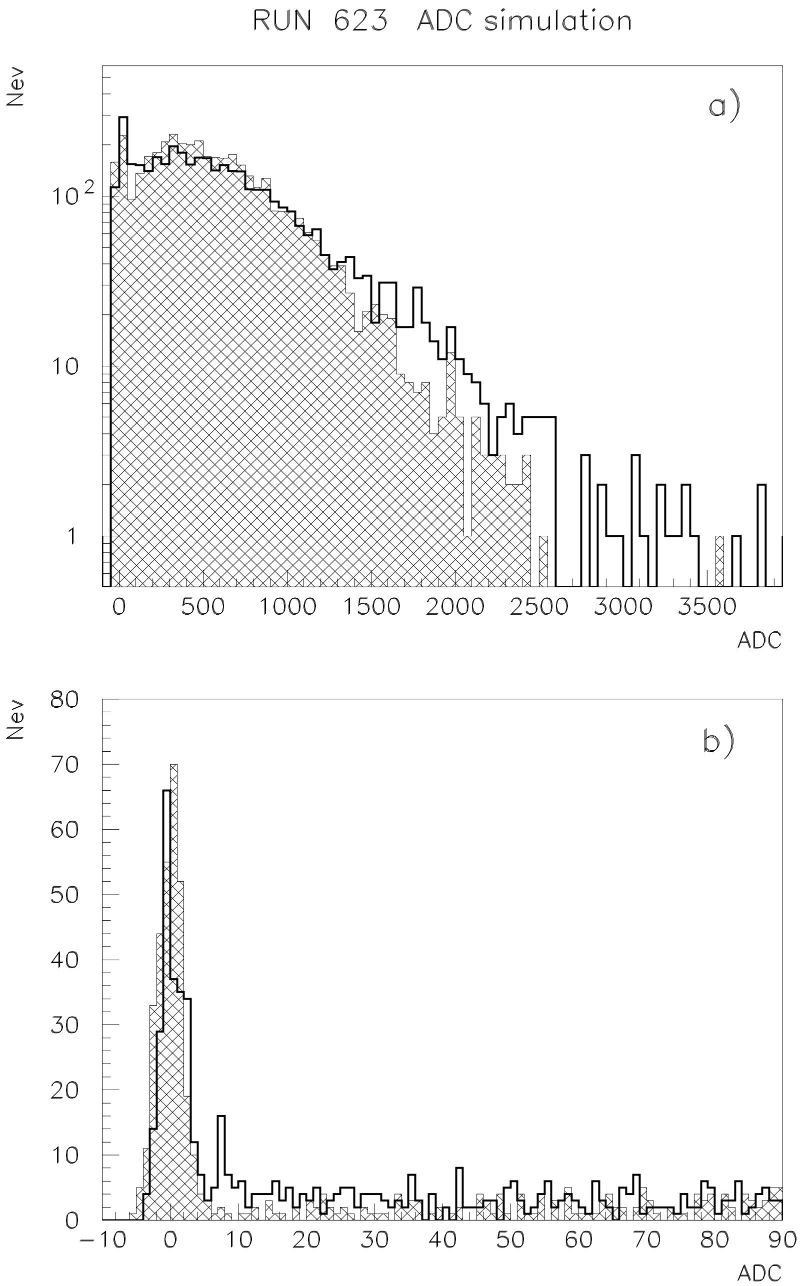

Figure 7: Comparison of measured ADC distribution and predicted by EGS4 MC (hatched histogram).

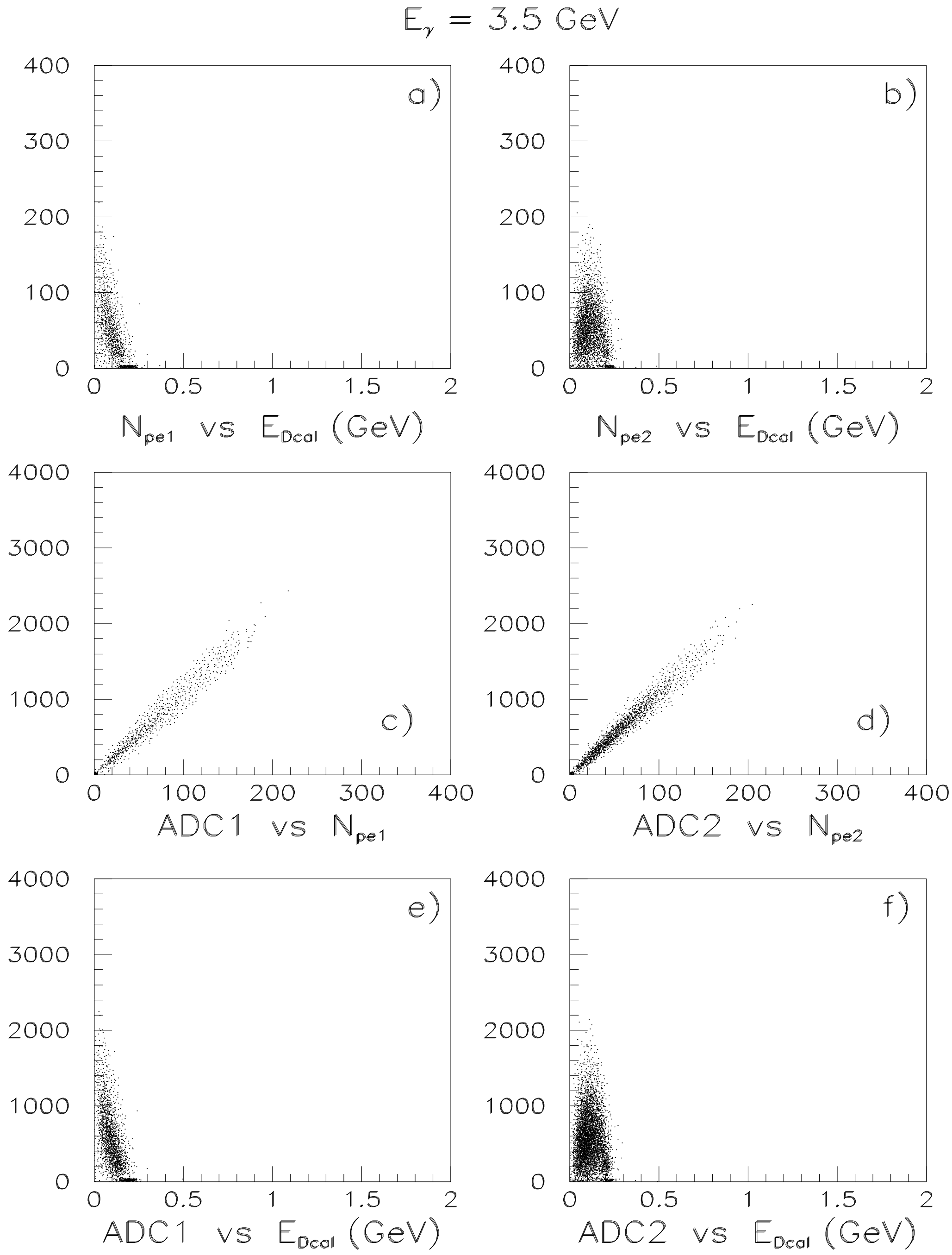

Figure 8: Correlation between the number of photons, corresponding ADC's and detected energy in the calorimeter by Geant MC for the generated energy 3.5 GeV.

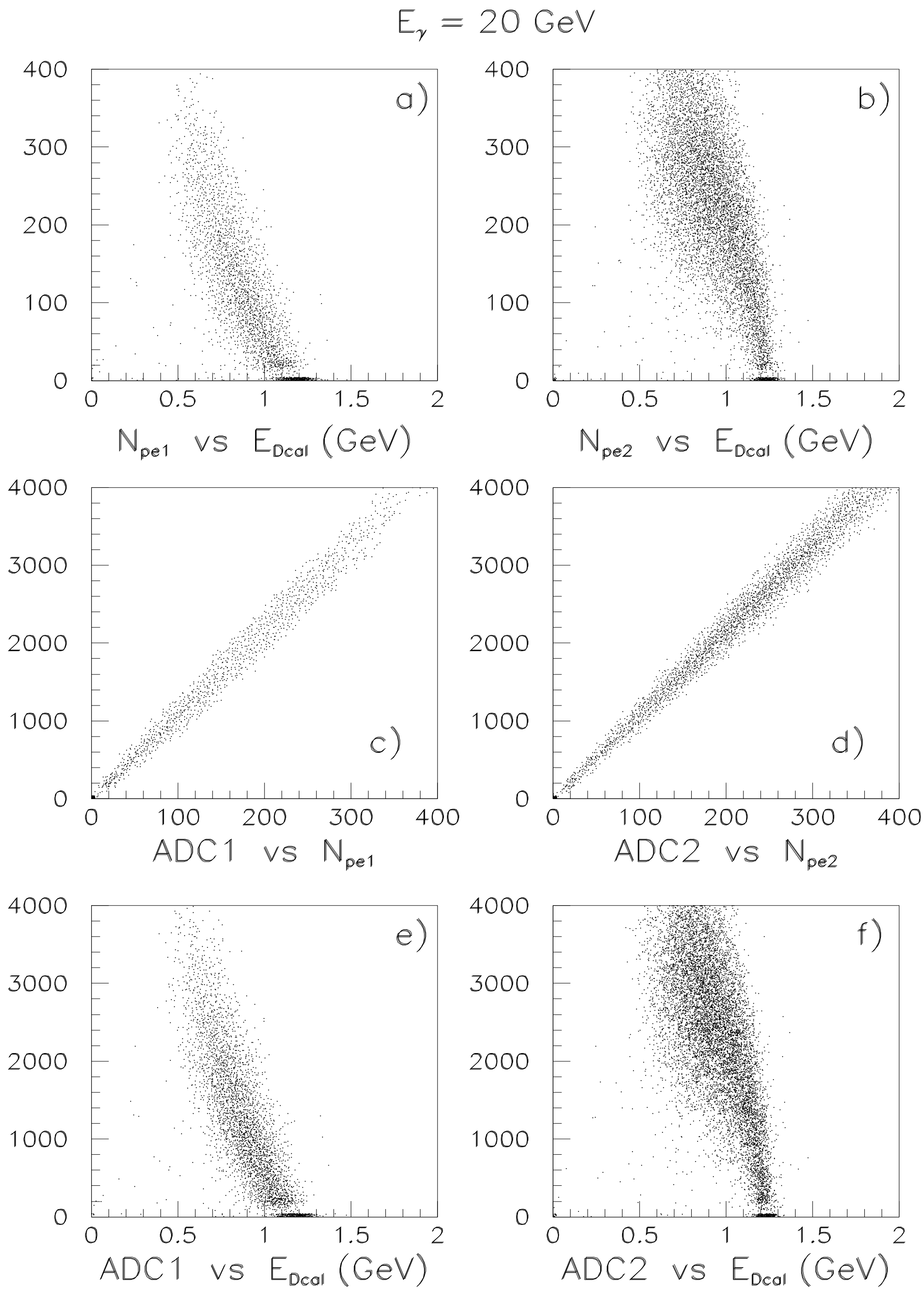

Figure 9: Correlation between the number of photons, corresponding ADC's and detected energy in the calorimeter by Geant MC for the generated energy 20 GeV.

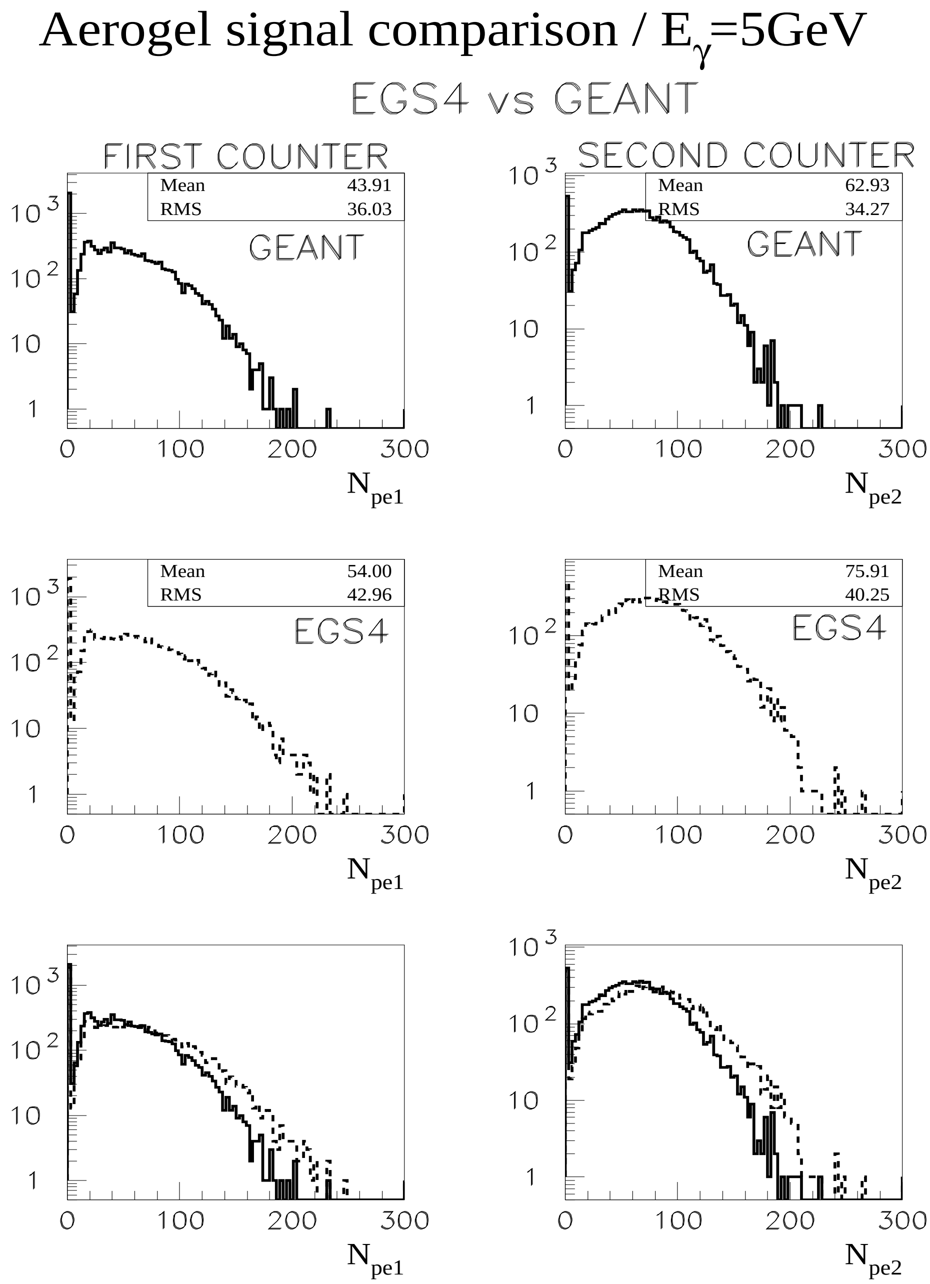

Figure 10: The comparison of the distributions of the number of photo-electrons generated in first (left column histograms) and in second (right column histograms) aerogel stacks. Geant and EGS4 MC results are shown separately and their comparison is shown in bottom raw histograms. The generated photon energy = 5 GeV.

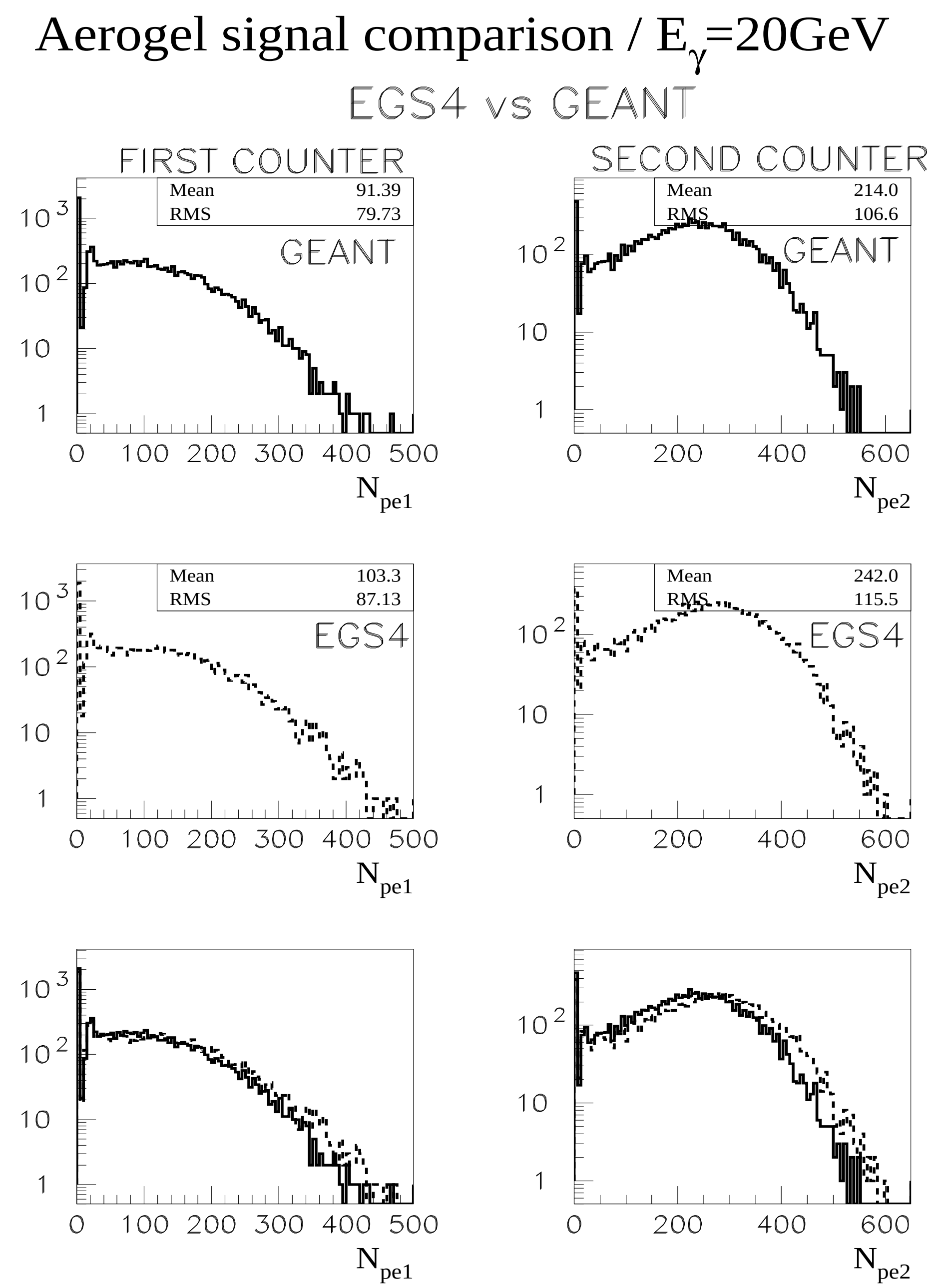

Figure 11: Same as in Fig.10. The generated photon energy is 20 GeV.

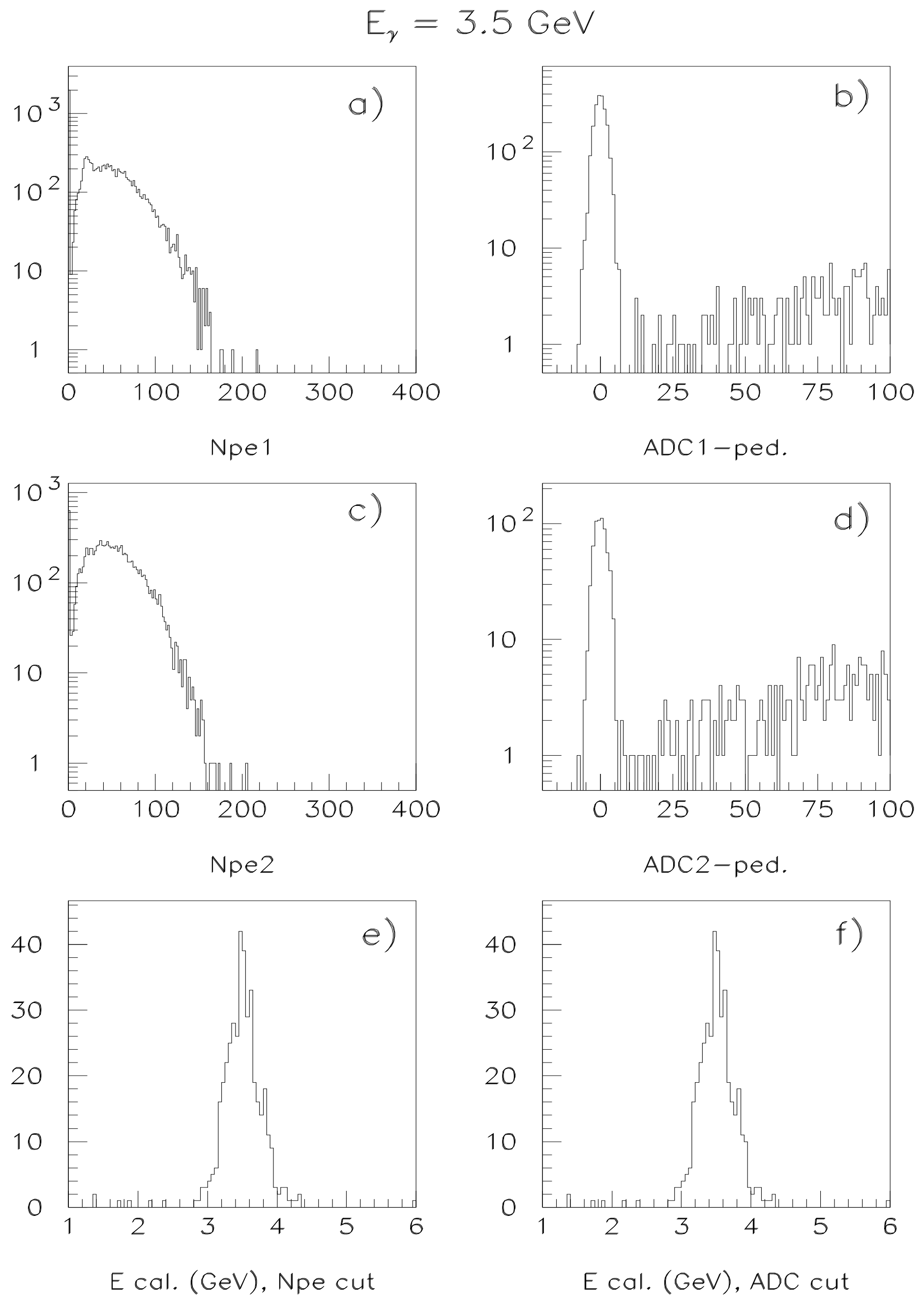

Figure 12: Distributions of the photo-electrons, the corresponding ADC's in both aerogel stacks and the energy deposit in the calorimeter for 3.5 GeV generated bremsstrahlung photon.

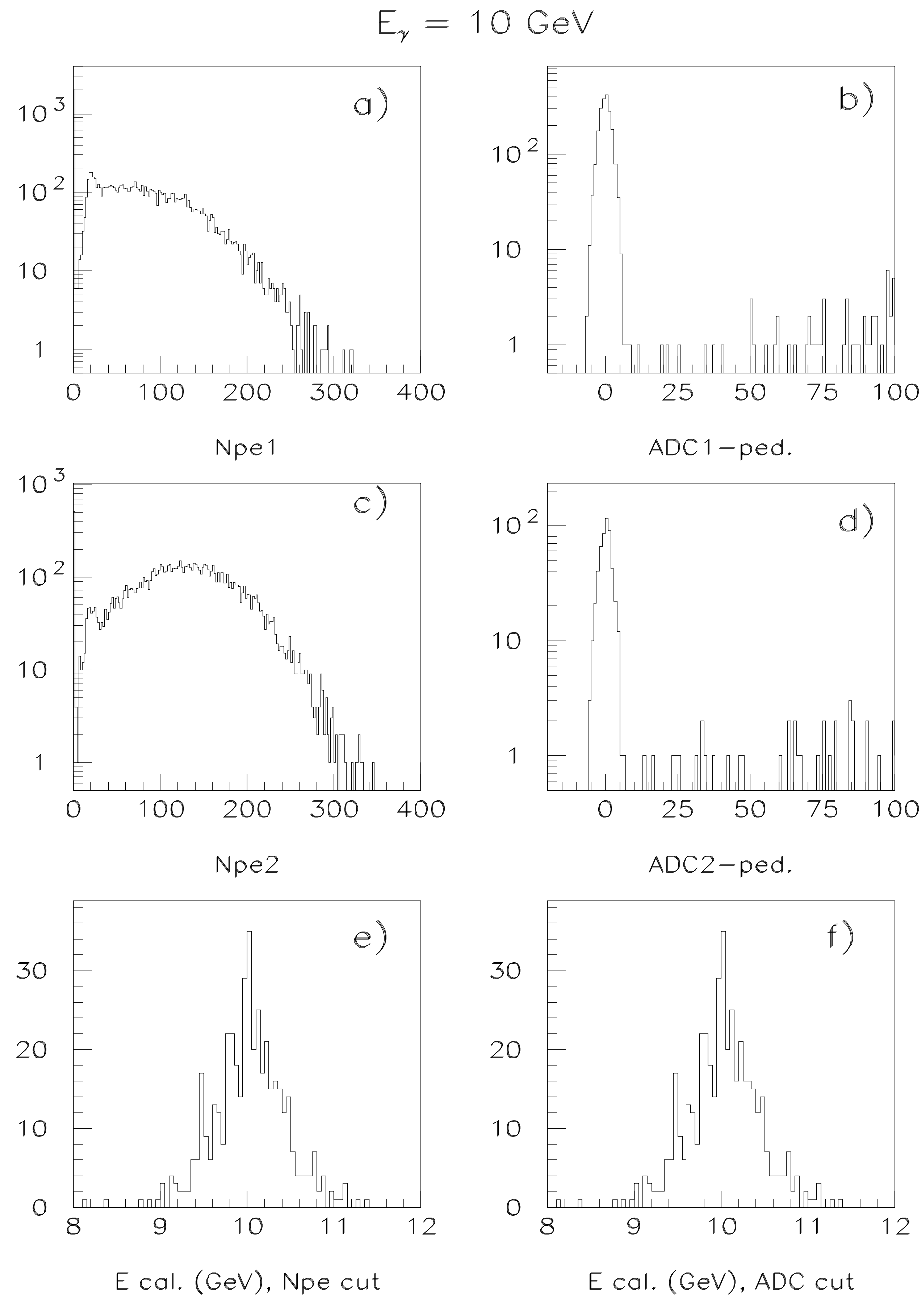

Figure 13: Distributions of the photo-electrons, the corresponding ADC's in both aerogel stacks and the energy deposit in the calorimeter for 10 GeV generated bremsstrahlung photon.

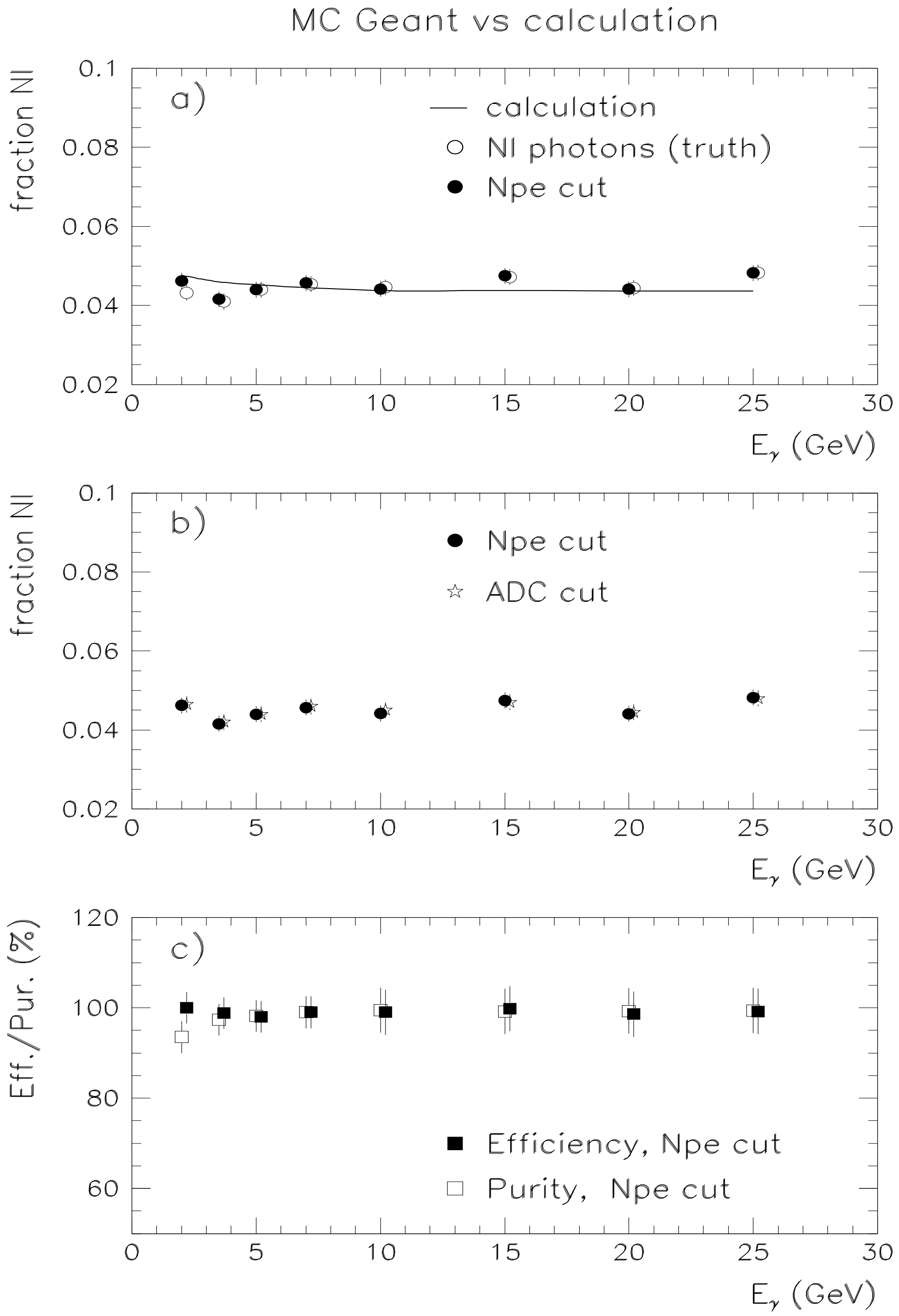

Figure 14: Comparison of three methods of identifying the non-interacting photons - a), b). Fig. c) shows the efficiency and purity of the sample of non-interacting photons selected on the basis of the absence of the photo-electrons.

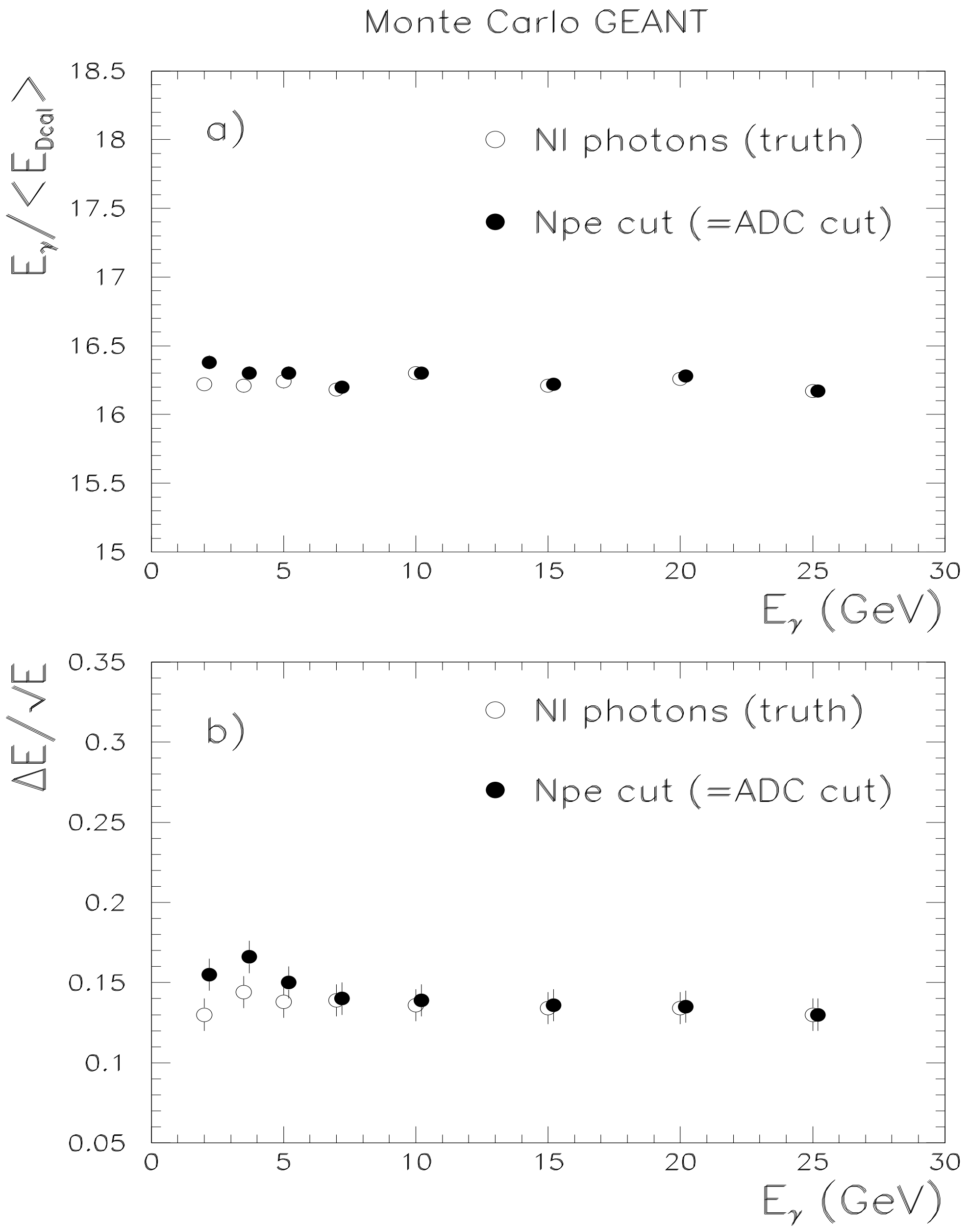

Figure 15: a) The " calibration constant ", b) the " resolution " $\Delta E/\sqrt{E}$ for the NI photons.

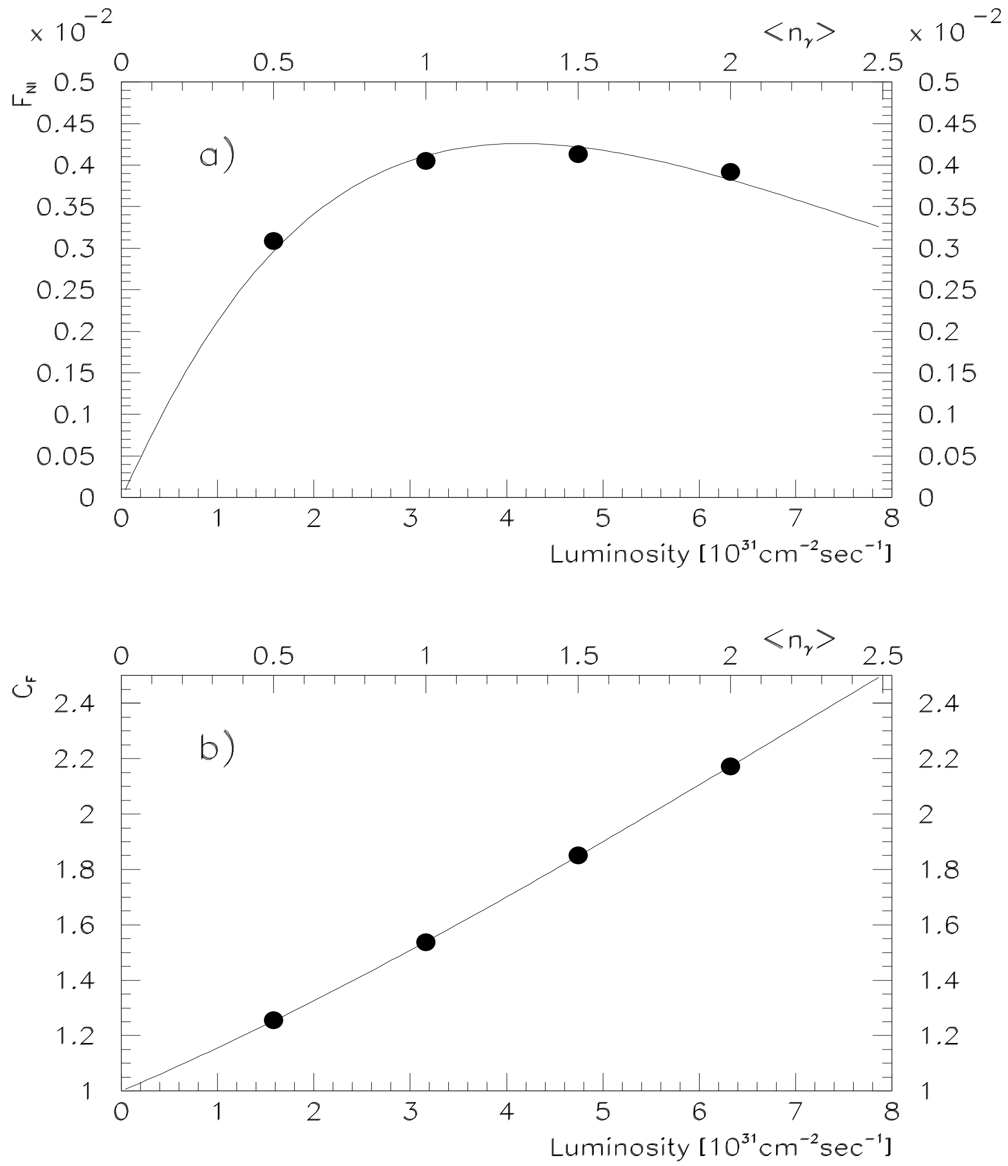

Figure 16: F_{NI} and C_F for $E_\gamma > 5$ GeV as a function of $< n_\gamma >$ (see text). Curves are drawn to guide the eye. (F_{NI} - fraction of bcr with a non-interacting photon, C_F - correction factor for pile-up effects for different luminosities for trigger ($E_{TR} = 5$ GeV)).

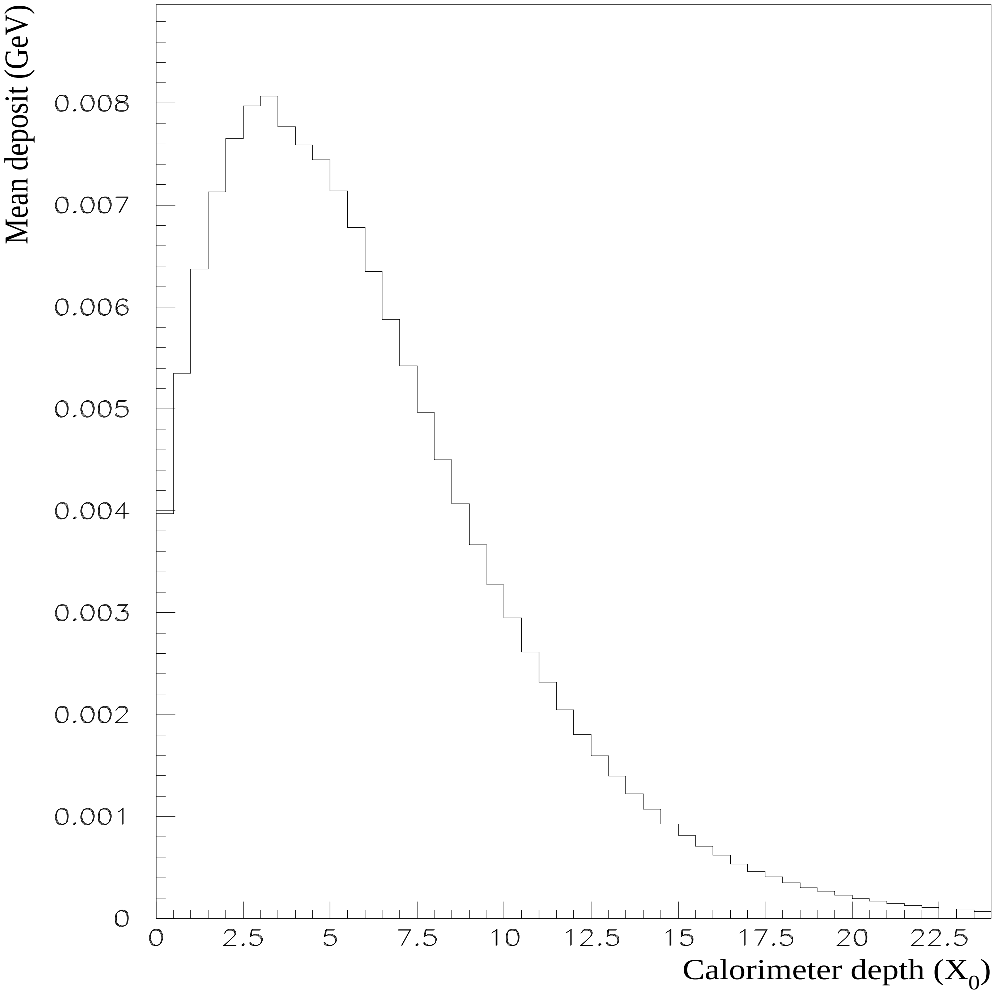

Figure 17: Energy deposits in the γ-calorimeter scintillators assuming bremsstrahlung spectrum for incident photons.

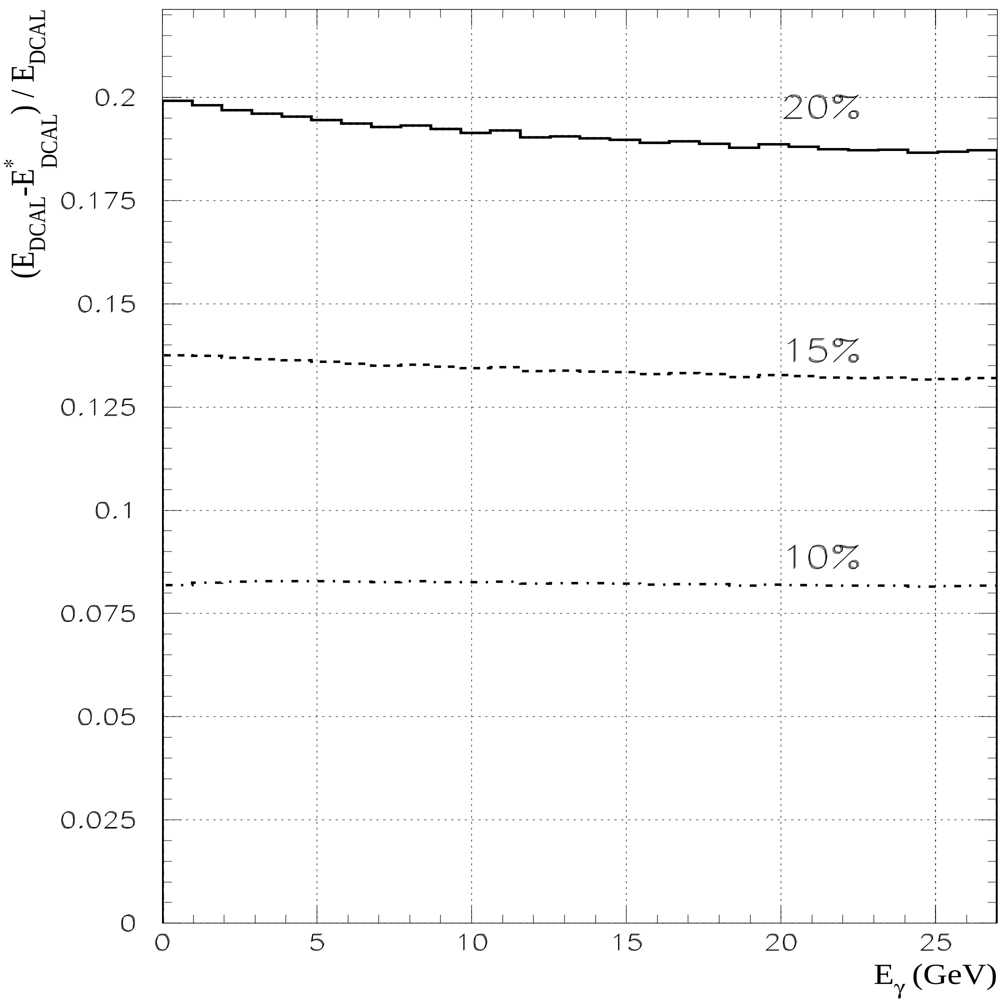

Figure 18: The impact of the radiation damage of scintillators close to the cascade maximum on the calorimeter deposit measurement. E_{Dcal} - undamaged scintillators, E^{*}_{Dcal} - radiation damaged scintillators. The level of damage maximal of 10%, 15%, 20%.

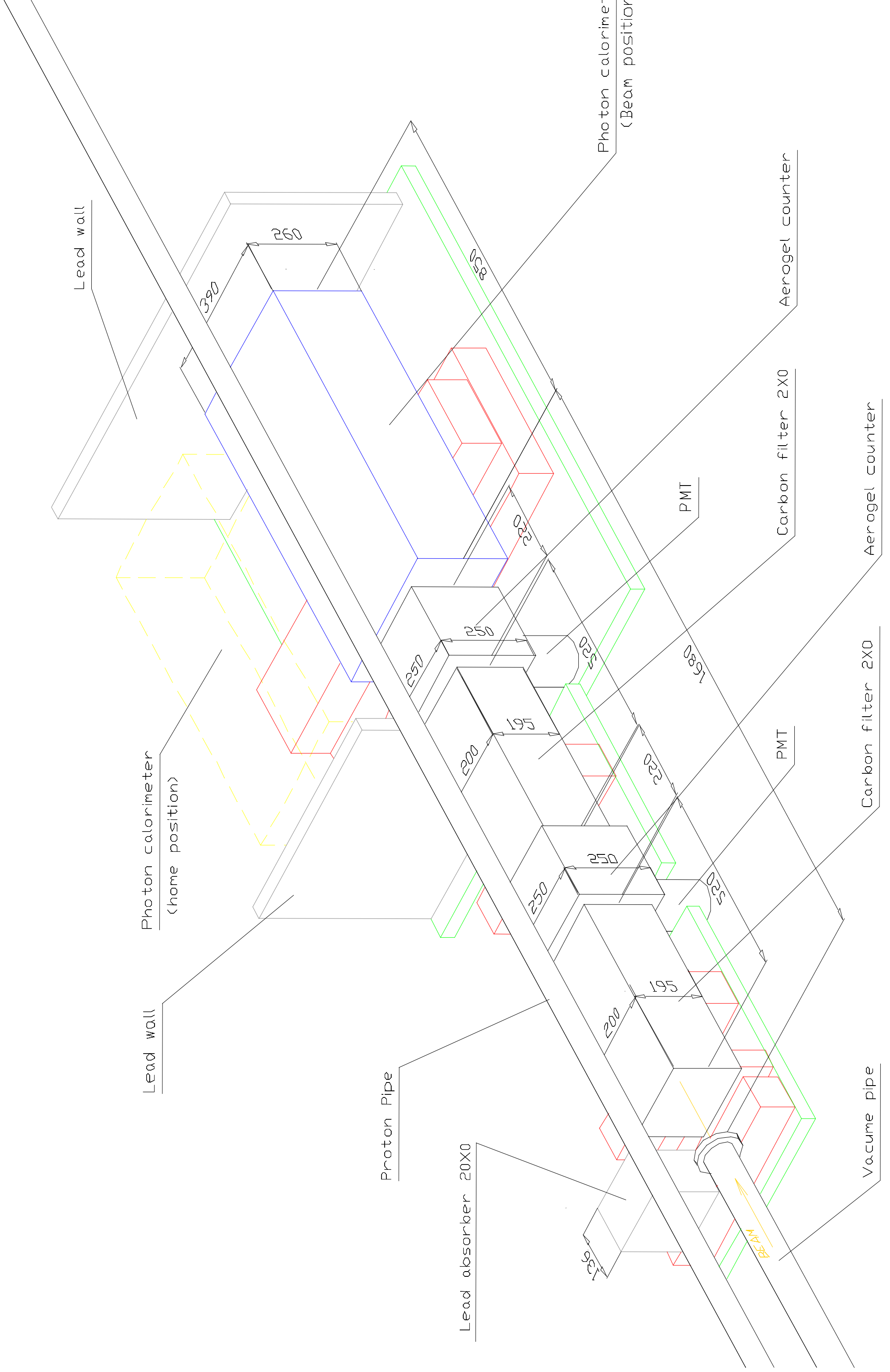

Figure 19: The overview of the proposed upgraded monitor.

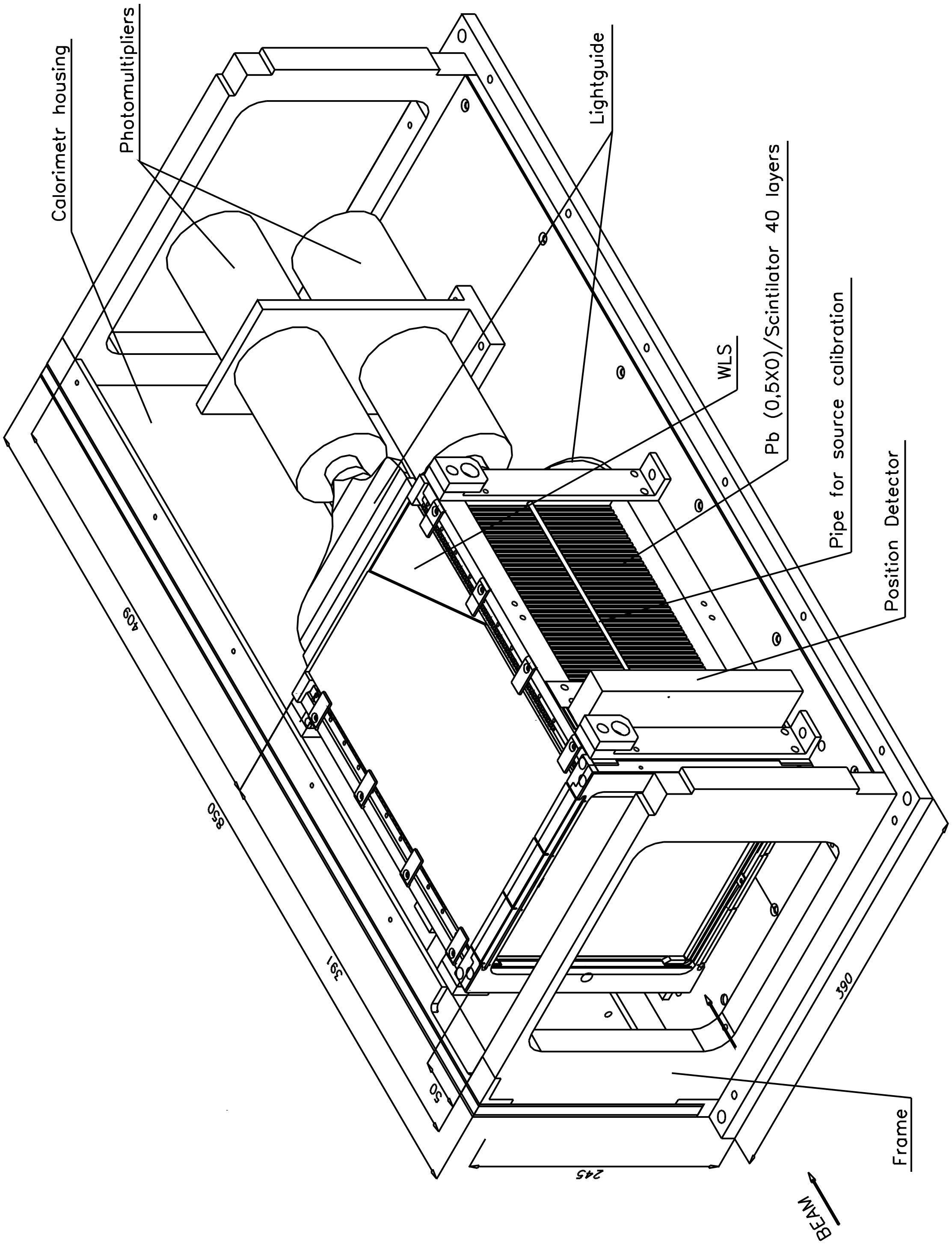

Figure 20: The general view of the upgraded photon calorimeter.

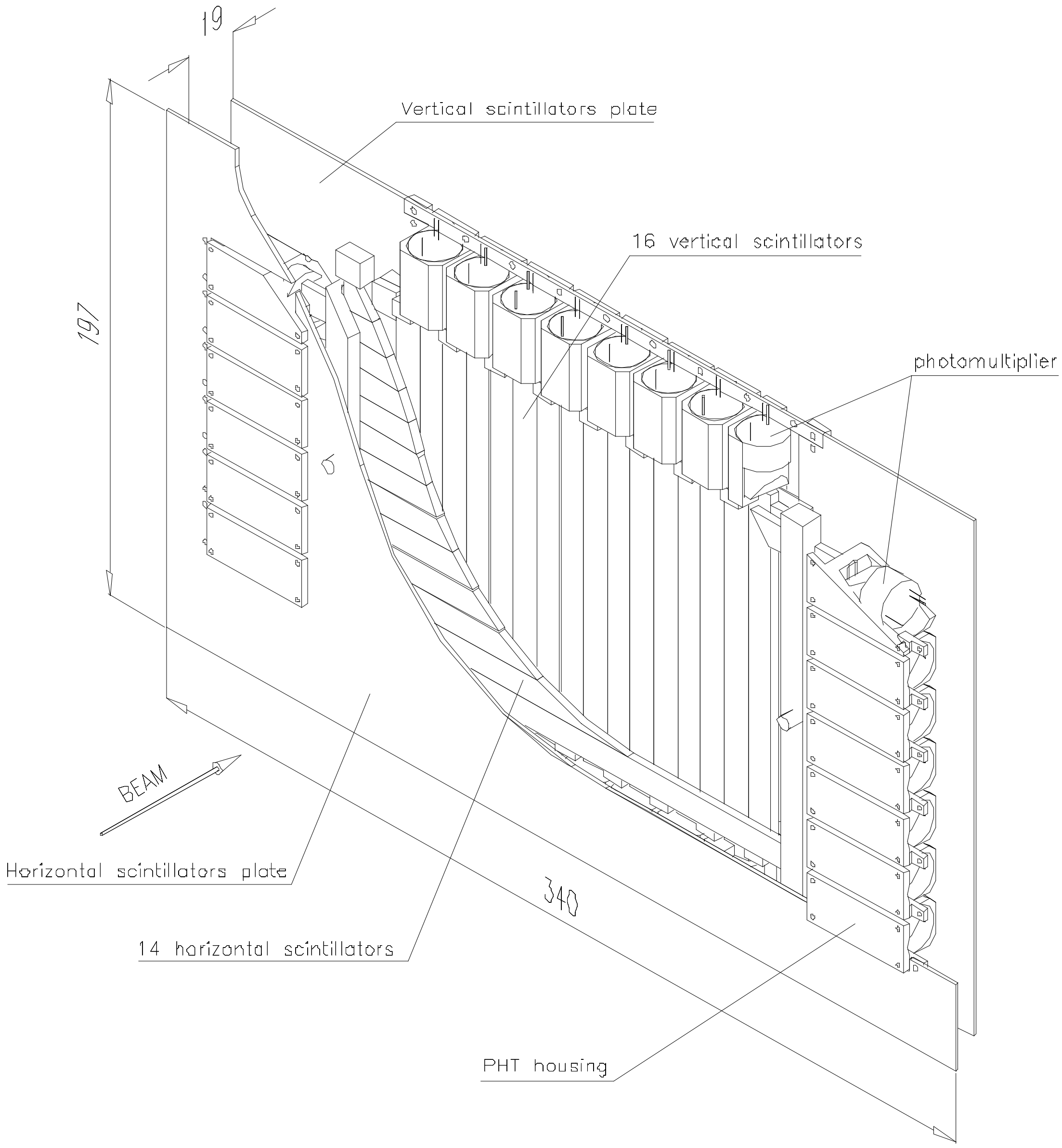

Figure 21: The overview of the position detector.

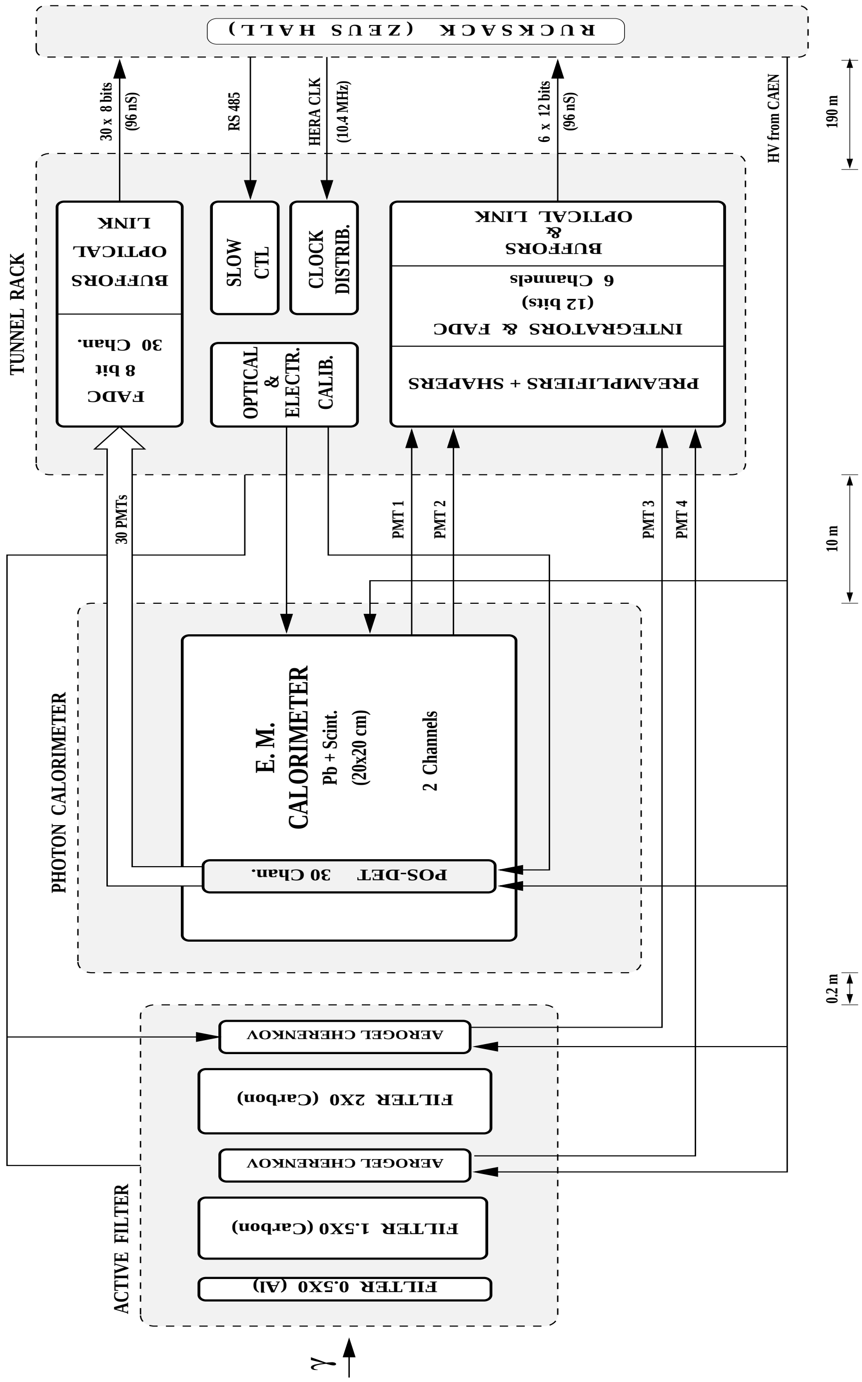

Figure 22: Block diagram of the read-out electronics.

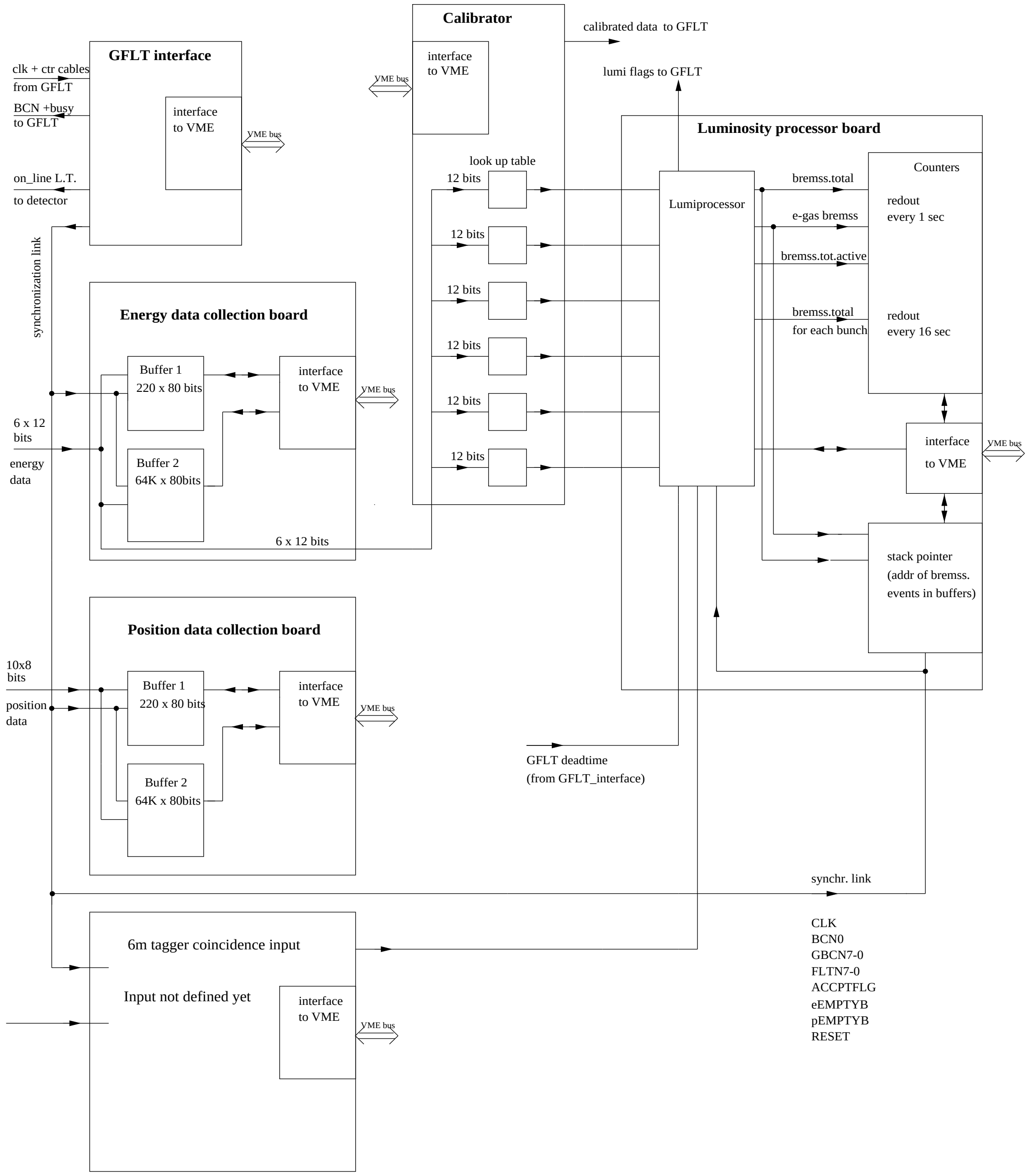

Figure 23: Block diagram of DAQ electronics.

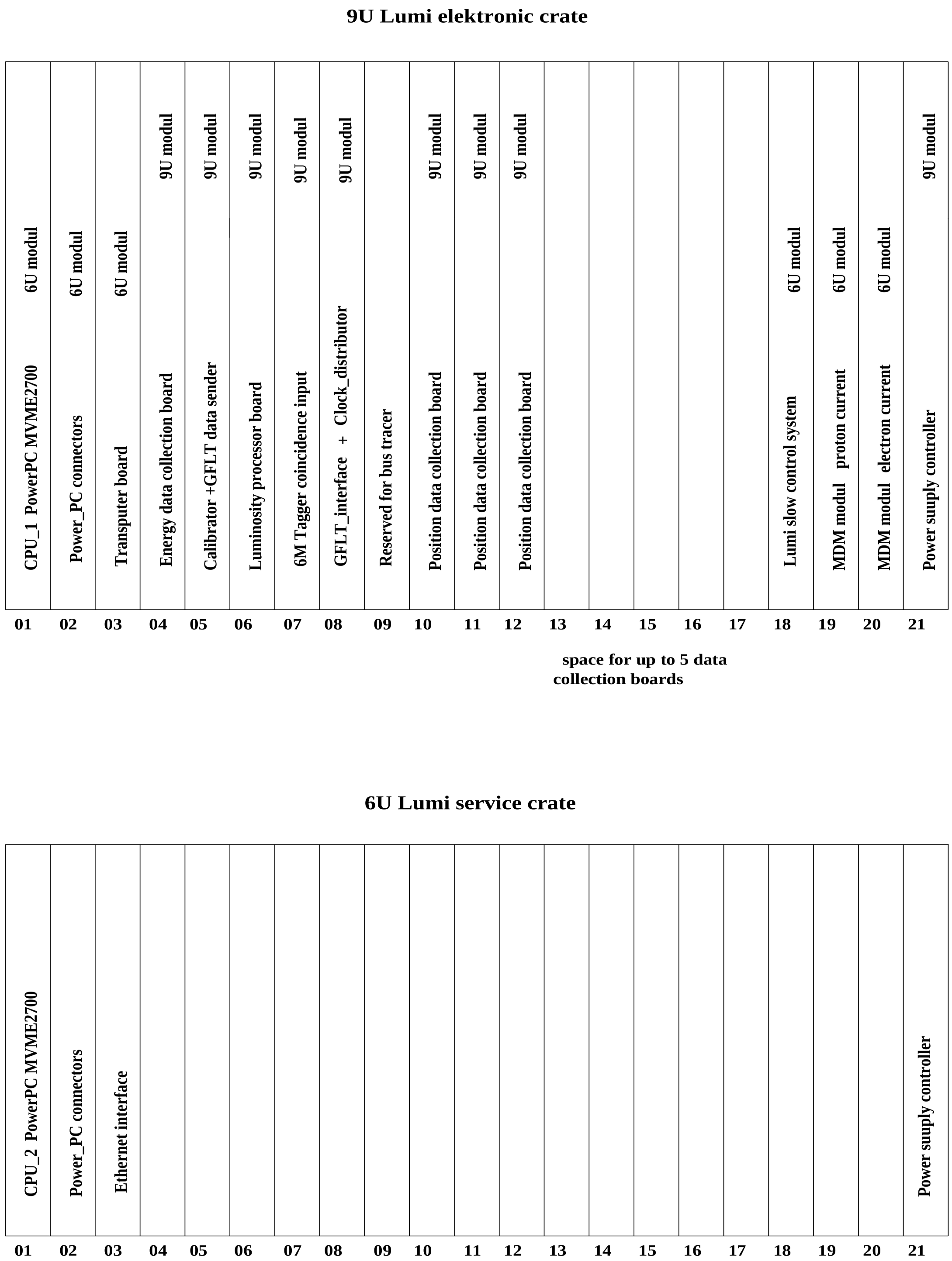

Figure 24: DAQ boards in rucksack.

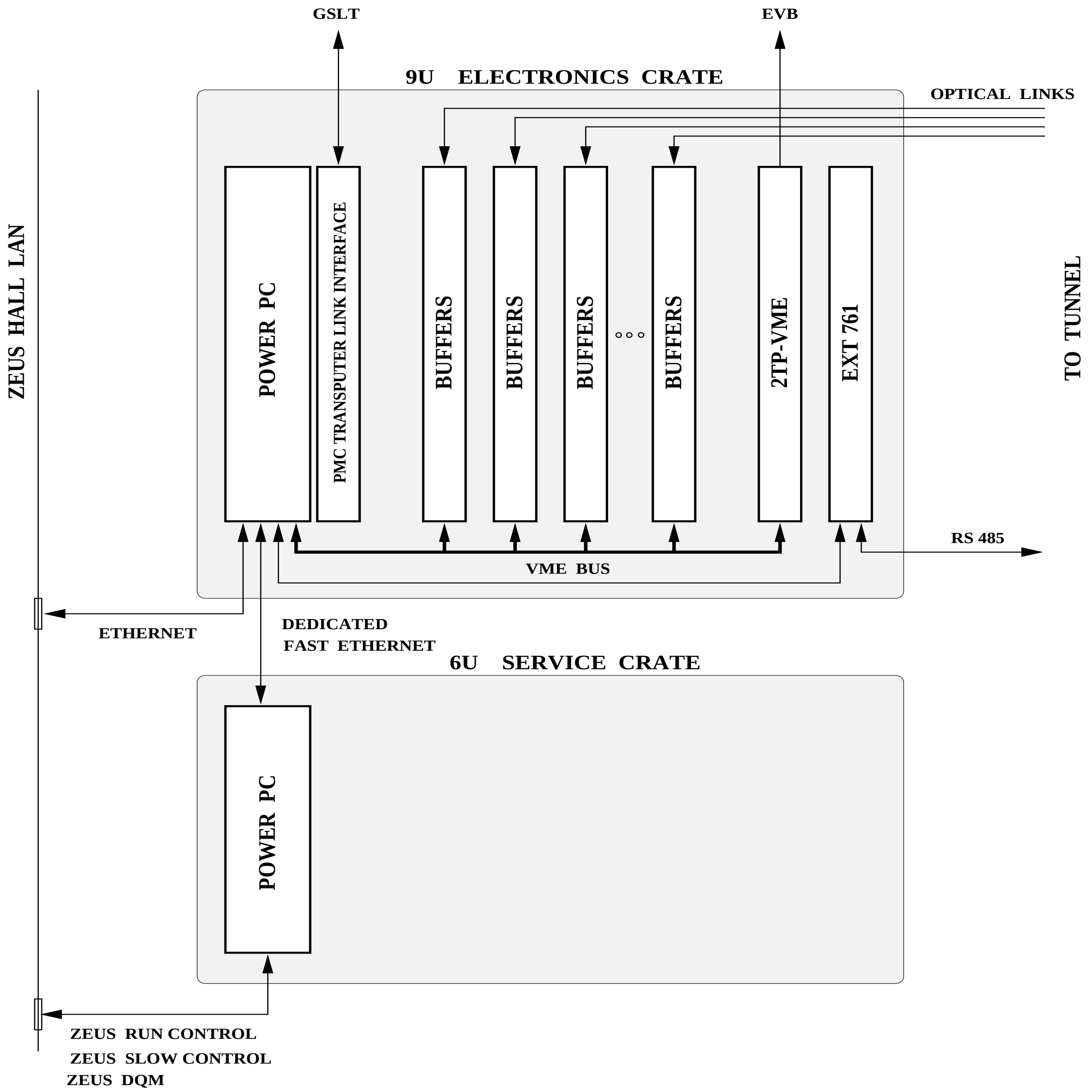

Figure 25: The VME environment contains 2 PowerPC hosts connected by fast ethernet. The service crate CPU is used to calculate online luminosity, to interface the Run Control System whereas the electronics crate CPU is used for data collection from hardware buffers, for communication with the GSLT via transputer links, and for data transfer to the EVB via 2TP_VME TripplePort Memory.

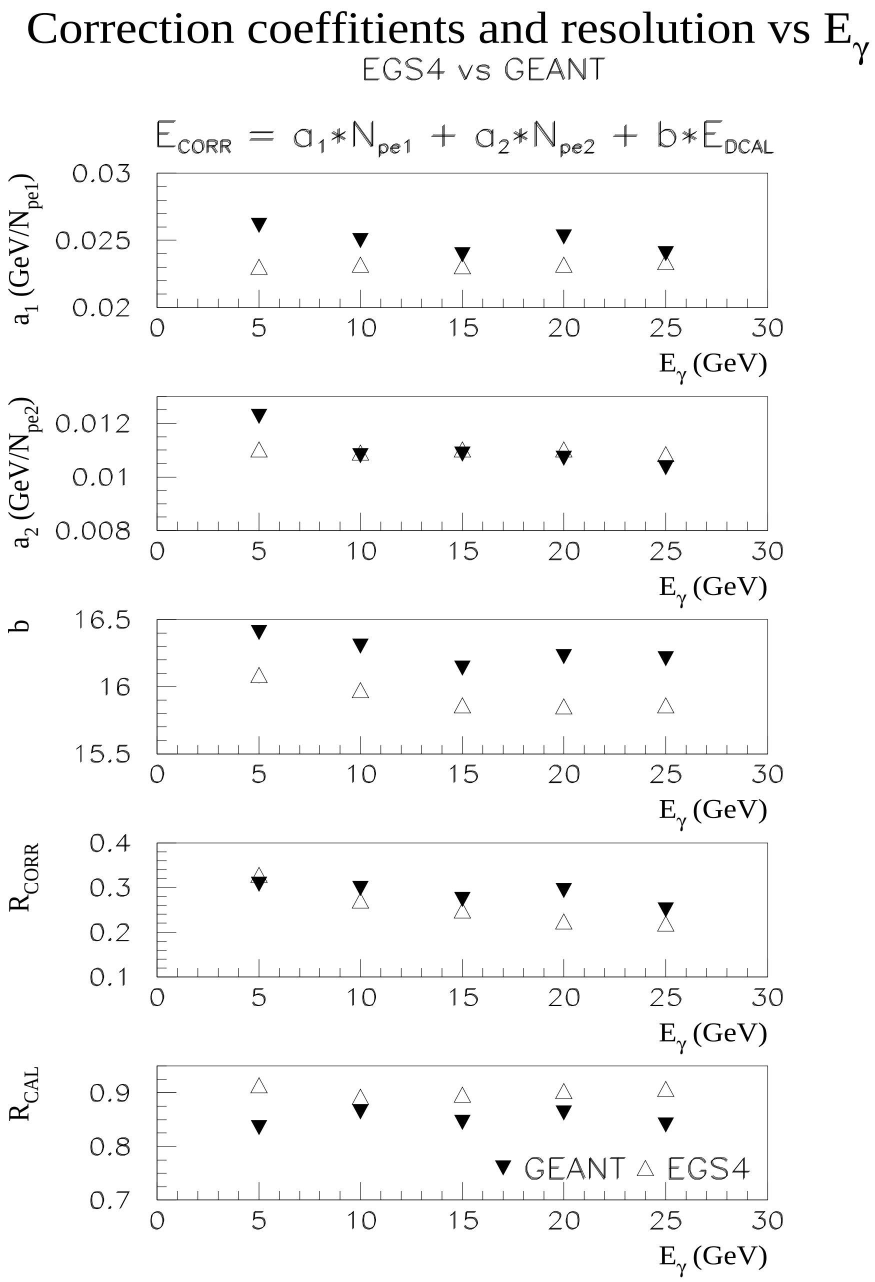

Figure 26: Comparison of Geant and EGS4 MC's simulations for corrected and uncorrected energy measurement in the calorimeter. R stands for $\Delta E/\sqrt{E}$.

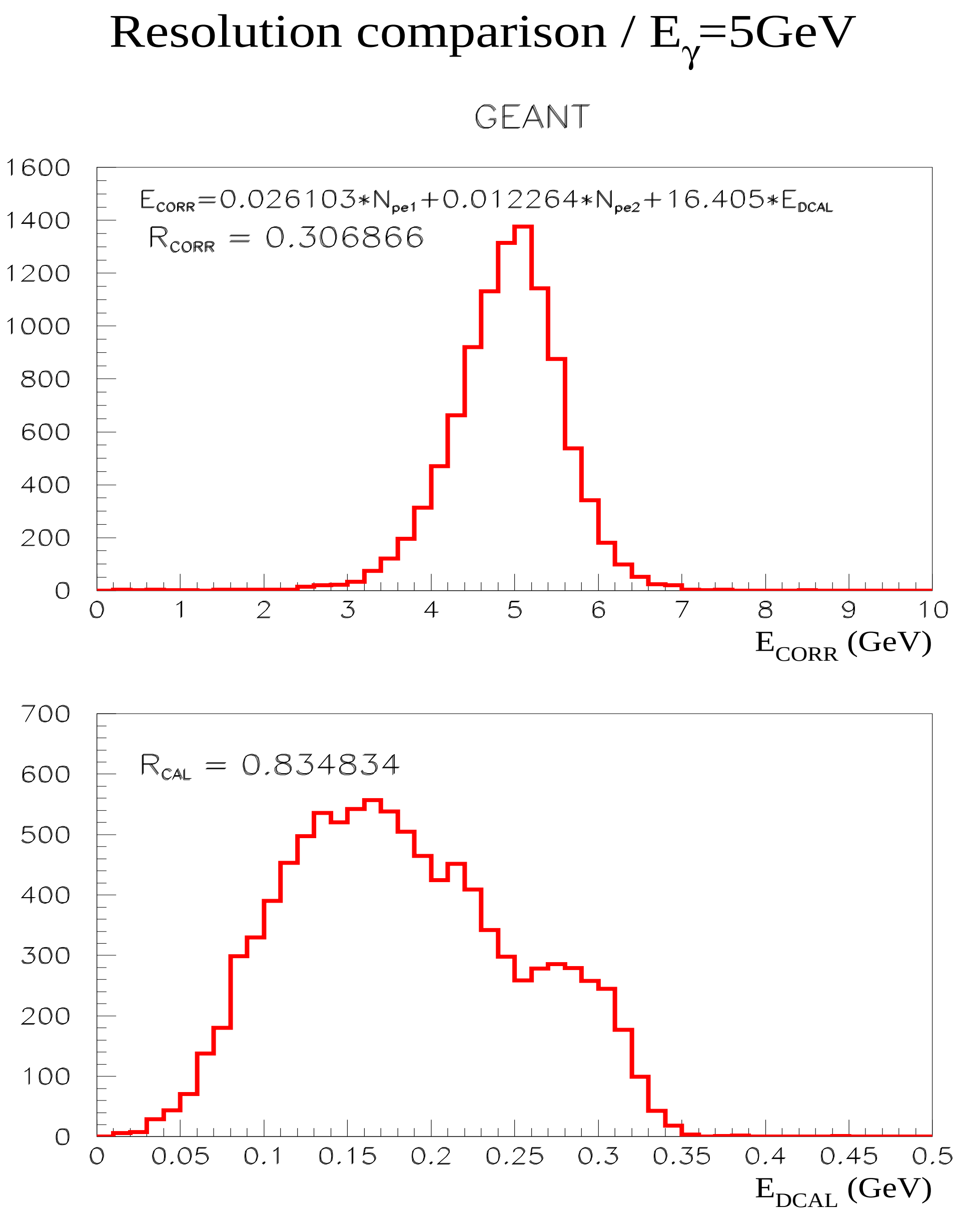

Figure 27: Comparison of the deduced energy resolution using the corrected (upper plot) and uncorrected (lower plot) energy deposits in the calorimeter. The plots are for 5 GeV photons - see text for explanation.

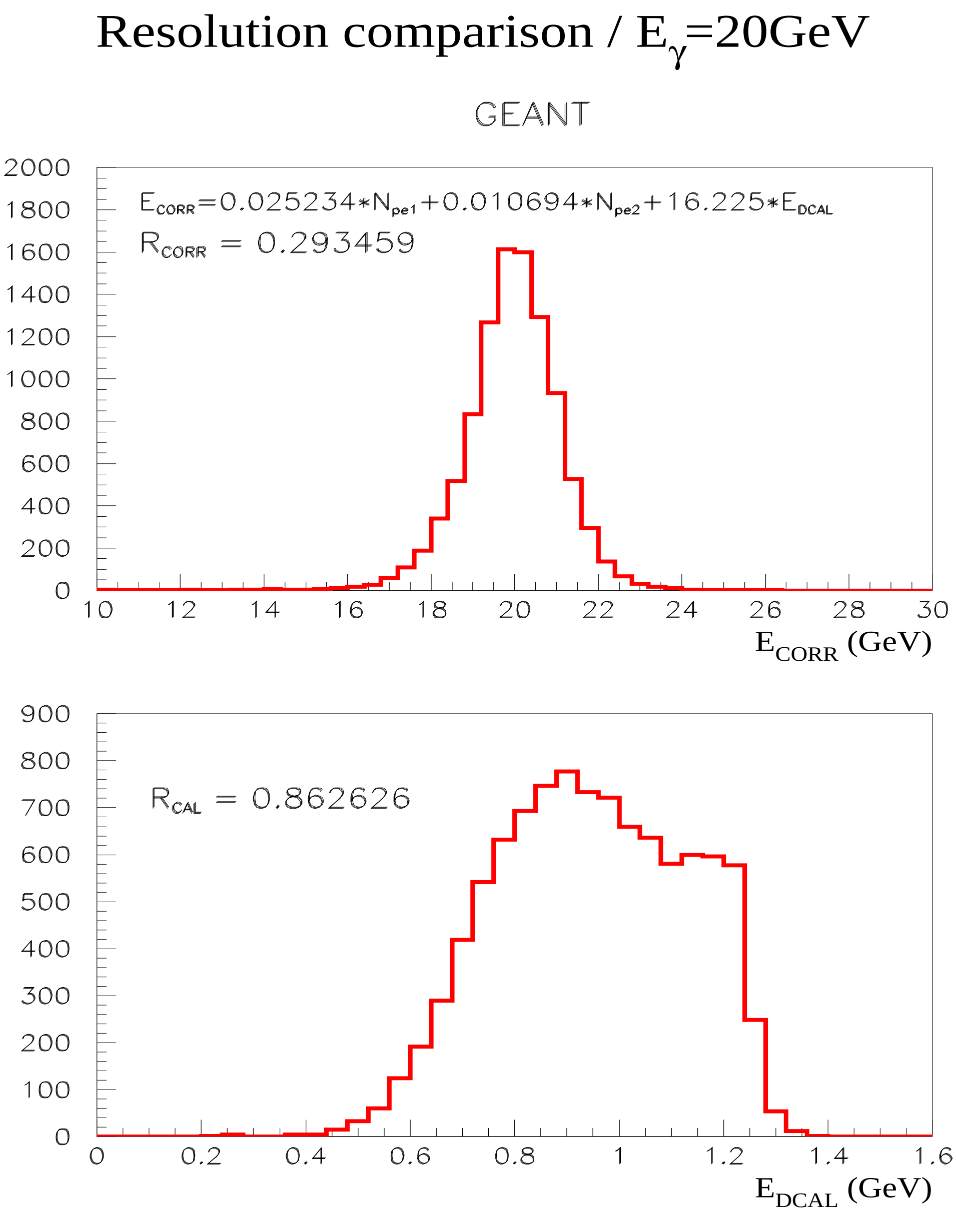

Figure 28: Same as Fig.27 for 20 GeV photons.

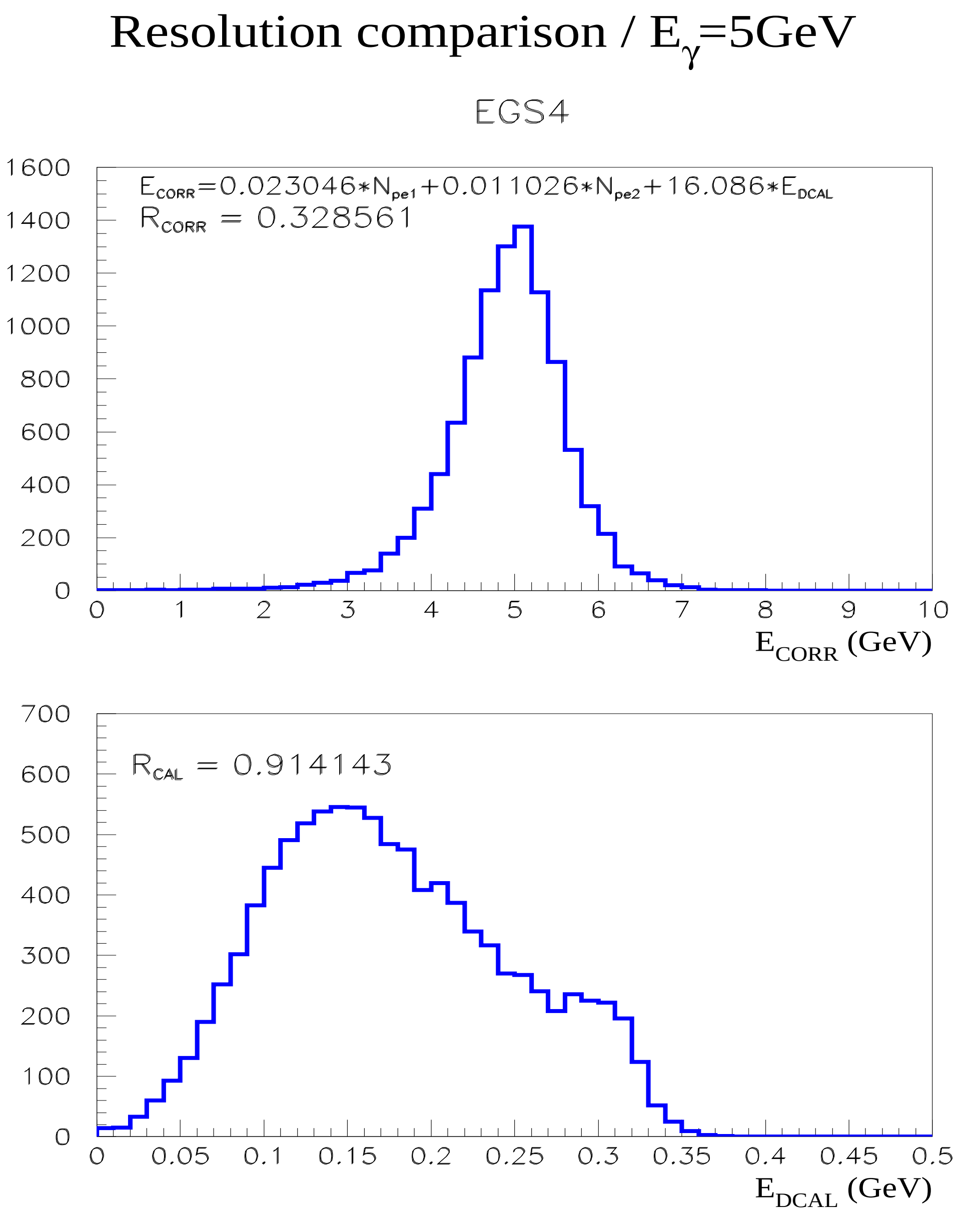

Figure 29: Same as Fig.27 but obtained with EGS4.

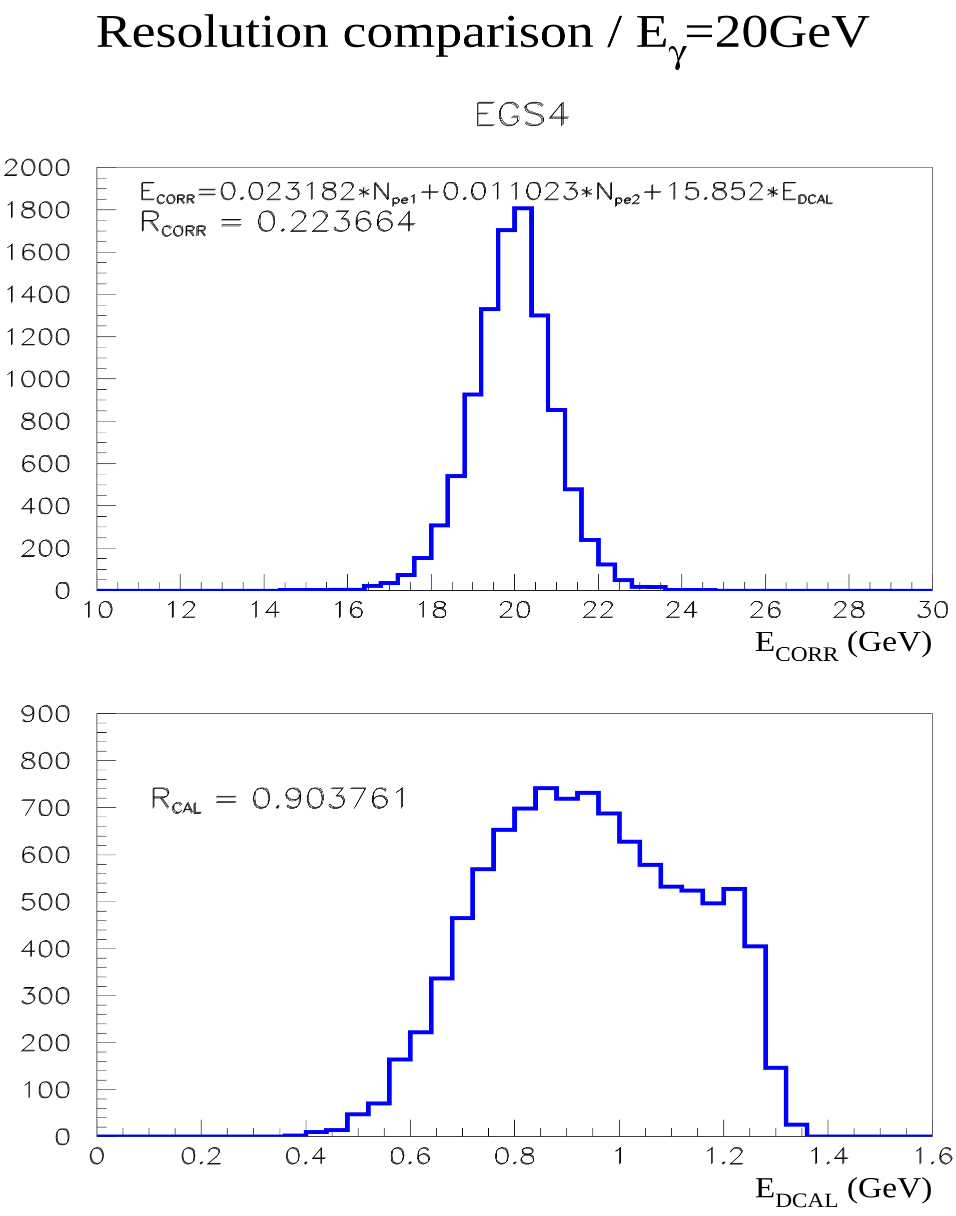

Figure 30: Same as Fig.28 but obtained with EGS4.

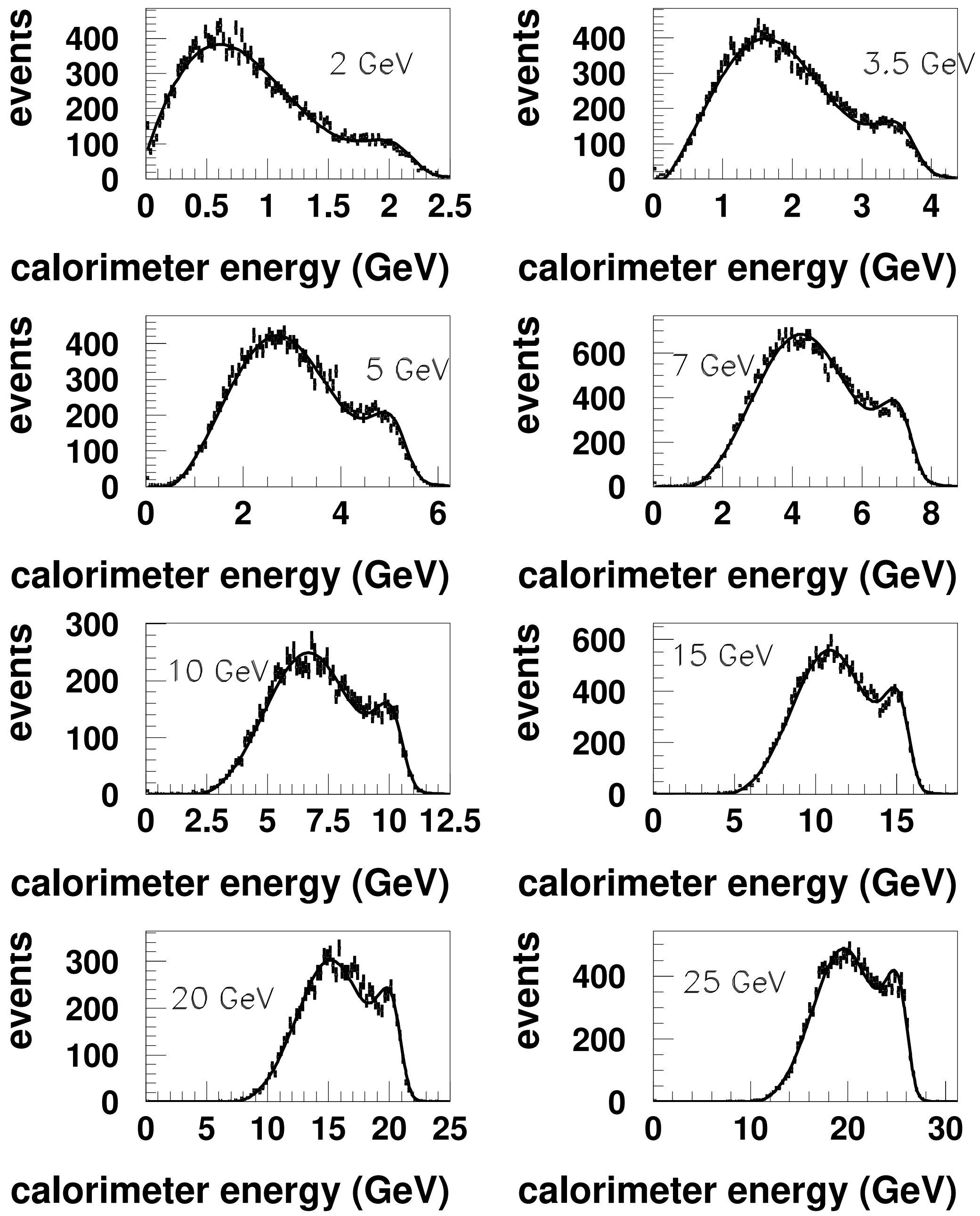

Figure 31: The simulated calorimeter energy distribution (points) for several incident photon energies. Lines represent fit to the distributions.

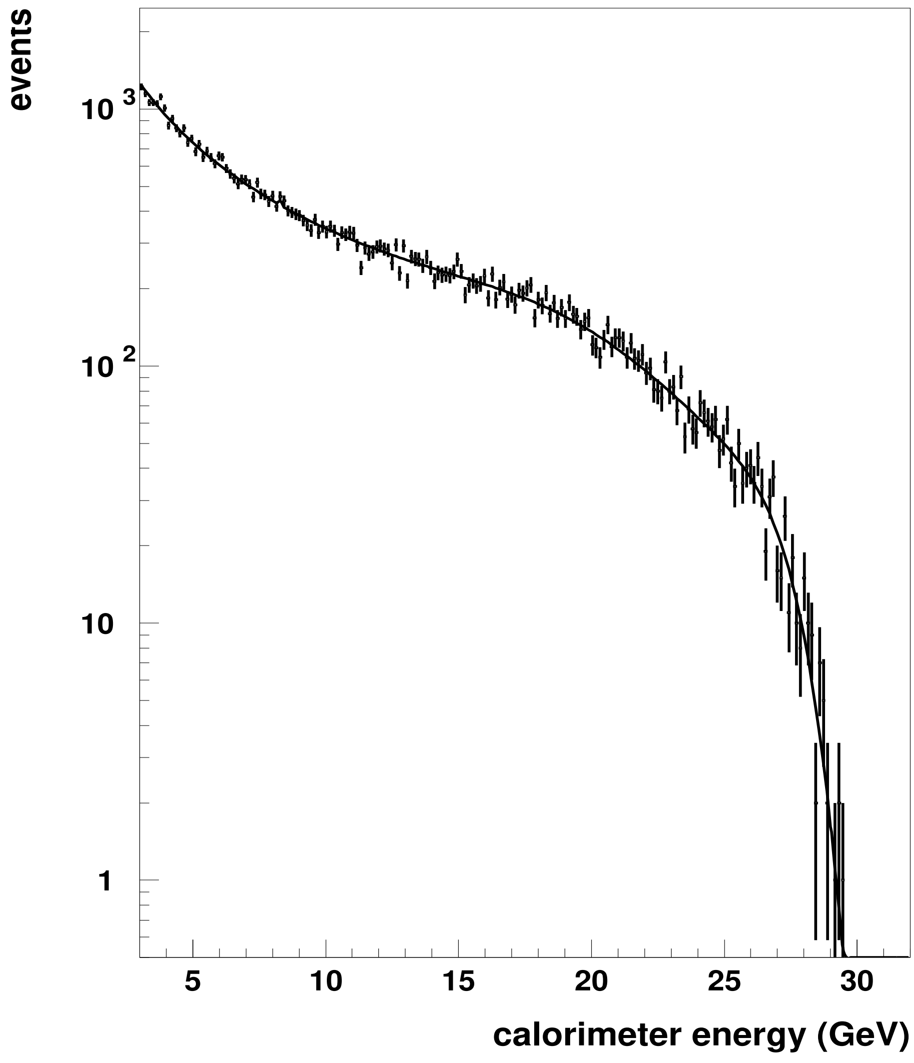

Figure 32: The simulated calorimeter energy distribution for e-gas bremsstrahlung photons (points). The solid line represents fit to the spectrum.

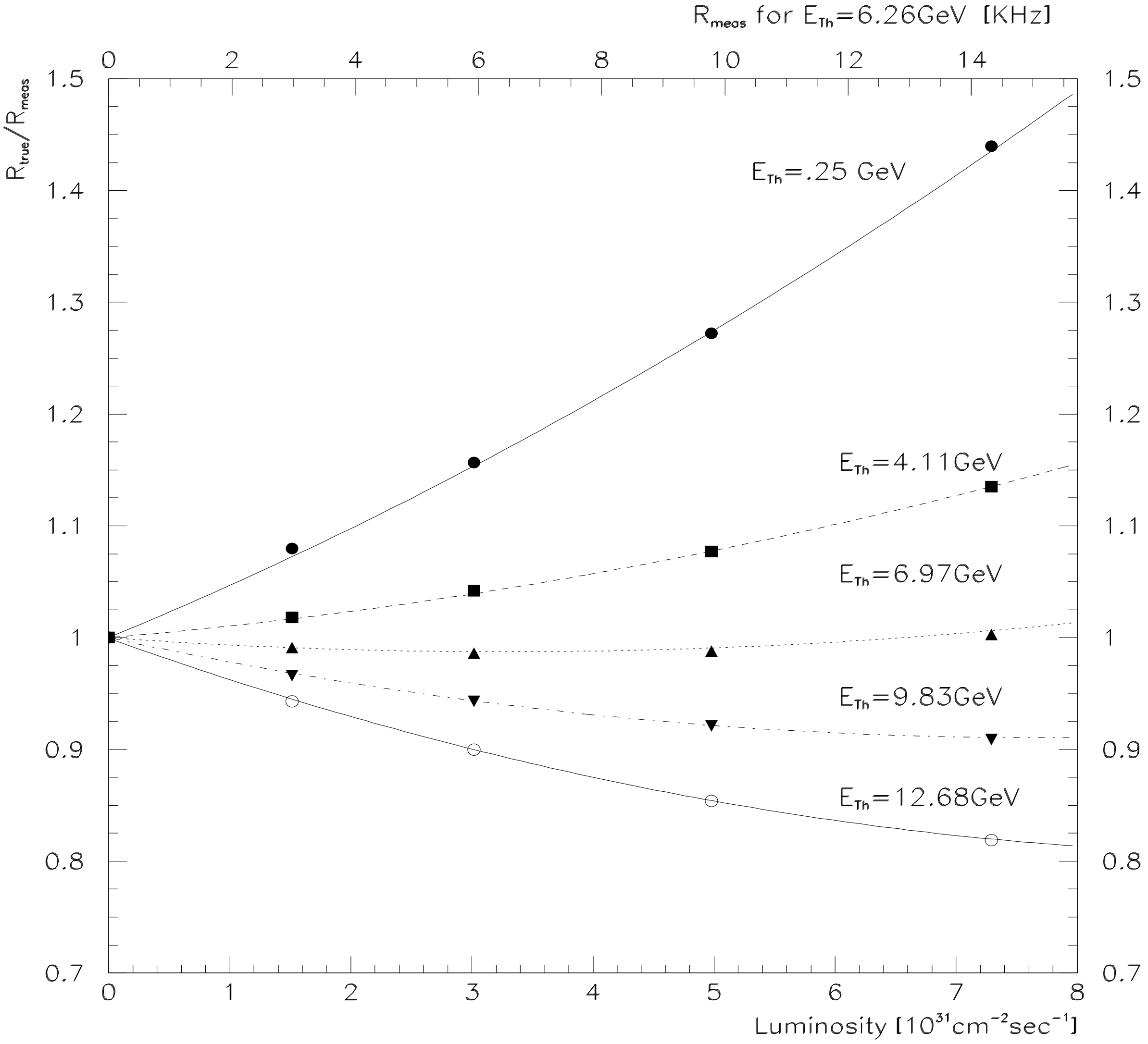

Figure 33: The different curves are drawn for the different energy thresholds E_T. The threshold energy is the minimum energy seen by the calorimeter. The corresponding number of ADC channels depend of course on the FADC counters used.